Published for SISSA by Springer

Received: November 30, 2023
Revised: February 6, 2024
Accepted: March 1, 2024
Published: March 20, 2024

Probing light quark Yukawa couplings through angularity distributions in Higgs boson decay

Bin Yan[a,b] **and Christopher Lee**[b]

[a]*Institute of High Energy Physics, Chinese Academy of Sciences, Beijing 100049, China*
[b]*Theoretical Division, Los Alamos National Laboratory, P.O. Box 1663, MS B283, Los Alamos, NM 87545, U.S.A.*

E-mail: yanbin@ihep.ac.cn, clee@lanl.gov

Abstract: We propose to utilize angularity distributions in Higgs boson decay to probe light quark Yukawa couplings at e^+e^- colliders. Angularities τ_a are a class of 2-jet event shapes with variable and tunable sensitivity to the distribution of radiation in hadronic jets in the final state. Using soft-collinear effective theory (SCET), we present a prediction of angularity distributions from Higgs decaying to quark and gluon states at e^+e^- colliders to NNLL + $\mathcal{O}(\alpha_s)$ accuracy. Due to the different color structures in quark and gluon jets, the angularity distributions from $H \to q\bar{q}$ and $H \to gg$ show different behaviors and can be used to constrain the light quark Yukawa couplings. We show that the upper limit of light quark Yukawa couplings could be probed to the level of $\sim 15\%$ of the bottom quark Yukawa coupling in the Standard Model in a conservative analysis window far away from nonperturbative effects and other uncertainties; the limit can be pushed to $\lesssim 7-9\%$ with better control of the nonperturbative effects especially on gluon angularity distributions and/or with multiple angularities.

Keywords: Anomalous Higgs Couplings, Effective Field Theories of QCD, Higgs Properties

ArXiv ePrint: 2311.12556

Open Access, © The Authors.
Article funded by SCOAP[3].

https://doi.org/10.1007/JHEP03(2024)123

Contents

1 Introduction

After the discovery of the Higgs boson at the Large Hadron Collider (LHC) [1, 2], precision measurements of the properties of the Higgs and proving that the Higgs boson is indeed responsible for electroweak symmetry breaking and mass generation have become a forefront goal of high energy physics. Determining the Yukawa couplings of the Higgs boson to fermions is one of the avenues to verify the Standard Model (SM) of particle physics. Since the Yukawa couplings are completely determined by the fermion mass in the SM, i.e. $y_q = \sqrt{2}m_q/v$ with $v = 246$ GeV, it is virtually impossible to probe the light quark Yukawa couplings directly due to the smallness of their mass. But these light quark Yukawa couplings may receive large modifications from new physics (NP) beyond the SM [3], and thus these NP effects could be probed by careful measurements of the Yukawa couplings.

Due to the large QCD backgrounds for the hadronic decay of Higgs boson at the LHC, a direct measurement of the light quark Yukawa couplings is challenging. Several approaches have been proposed to constrain the light quark Yukawa couplings indirectly. For example, one can measure the light quark Yukawa coupling through *i*) rare modes of Higgs boson decays, e.g. $h \to J/\Psi\gamma$ ($\phi\gamma$, $\rho\gamma$, $\omega\gamma$) [4–6]; *ii*) Higgs production in association with a charm-tagged jet [7]; iii) global analysis of the Higgs data [8–11]; *iv*) the transverse momentum (p_T) distribution of Higgs boson or jet in Higgs production processes [12–17]; *v*) the kinematic shapes of Higgs pair production [18], off-shell Higgs production [19, 20] and triple heavy vector boson production [21]; etc. The above proposals demand accurate calculations of light quark meson formation, charm tagging efficiency and faking rates of light quarks, or precise knowledge of the p_T spectrum of Higgs boson. Compared to hadron colliders, e^+e^- colliders provide direct access to all possible decay channels of the Higgs boson due to the clean

JHEP03(2024)123

environment. Several plans for future lepton colliders have been proposed, including the CEPC [22], ILC [23], CLIC [24] and FCC-ee [25]. Through the Higgs and Z boson associated production, the inclusive cross section could be measured to 0.5% accuracy at $\sqrt{s} = 250$ GeV with integrated luminosity of 5 ab^{-1} [22]. Such high accuracy of the total cross section offers a possibility to measure the light Yukawa couplings directly at the e^+e^- colliders.

The main difficulty of measuring the light quark Yukawa couplings at e^+e^- colliders is due to contamination from Higgs boson decays to gluons, obscuring jets initiated by light quarks. To suppress the gluon background, it is necessary to use some form of quark and gluon jet discrimination. A wide variety of quark and gluon discriminants have been proposed, e.g., in refs. [26–35]. To first approximation, the main underlying feature is that the initiating energetic quark radiates soft or collinear gluons in proportion to its color factor $C_F = 4/3$, while initiating hard gluons radiate additional gluons proportional to the factor $C_A = 3$, making gluon-initiated jets "broader" or more "diffuse" than quark-initated jets. Good discriminants tease out these and other more subtle differences between gluon and quark jets. Ideally, the discriminants have properties that can also be predicted reliably from first principles in QCD, though powerful methods also exist that are totally data-driven and require no input from QCD at all, e.g. [36].

One class of observables that can discriminate broad features of quark and gluon jets and can also be predicted to high accuracy in QCD are hadronic event shapes (e.g. [37–41]). Thus we explore in this paper their potential to constrain the light quark Yukawa couplings at e^+e^- colliders. Similar ideas have been discussed in ref. [42], e.g. event shapes including thrust [43], heavy hemisphere mass [44, 45], C parameter [46, 47], broadening [48] and Durham 2-to-3-jet transition parameter [49], and jet energy profile [50–53]. Ref. [42] showed that these event shapes can provide a much stronger sensitivity for the light quark Yukawa couplings compared to methods proposed for the LHC, e.g. $y_q < 0.091 y_b$ by event shapes for $q = u, d, s$ at 95% confidence level at CEPC [42], while it only can be constrained to $0.4 \sim 0.5 y_b$ by Higgs p_T spectrum at the LHC [12, 13], where y_b is the bottom quark Yukawa coupling in the SM. Recently, ref. [20] studied the potential of off-shell Higgs production to further improve the Yukawa coupling limit, projecting improvements of 20% or more compared to Higgs+jet production depending on assumptions about uncertainties on background.

Event shapes in e^+e^- collisions to hadrons have already been computed to very high accuracy, up to N^{3}LL$'$ resummed accuracy matched to NNLO fixed-order calculations, e.g. [38, 39, 41, 54]. Recently, theoretical predictions of event shape observables in Higgs boson decays have also been computed to high accuracy, e.g. the thrust distribution has been calculated to NLO accuracy plus NNLO singular terms [55], the energy-energy correlation from Higgs decaying to gluon mode has been computed to NLO accuracy [56]. Ref. [57] also computed the 2-jettiness distribution from the decay of the Higgs boson to a $b\bar{b}$ quark pair and to gluons, to NNLL$'$+NNLO accuracy and even approximate N^{4}LL accuracy in [58]. In this work, we propose to use a class of event shapes, *angularities* [59], to separate the $q\bar{q}$ channel from the gg channel in Higgs decays and to improve measurements of the light quark Yukawa couplings at lepton colliders. (The thrust and total jet broadening used in ref. [55] are special cases of the angularities.) We take advantage of recent results that make possible the prediction of angularity distributions to NNLL$'$ accuracy in resummed perturbation theory [60]. We also newly compute the LO fixed-order $\mathcal{O}(\alpha_s)$ corrections to general angularities in Higgs decay. We find that using any single angularity distribution

JHEP03(2024)123

allows determination of the light quark Yukawa couplings to similar or somewhat better precision as other individual event shapes studied in ref. [55], depending on whether we use a conservative analysis window at larger τ_a away from large nonperturbative effects and other corrections, yielding a potential bound of $y_q \lesssim 0.15 y_b$, or a more aggressive window that enters further into the nonperturbative region but thus takes advantage of the very different peaks for the quark and gluon angularity distributions, yielding $y_q \lesssim 0.7 - 0.9 y_b$. We also perform a very preliminary study using Pythia of the ability of double differential distributions of angularities to improve this reach further, attempting to utilize their additional power over single angularity distributions to distinguish quark and gluon jets. We find that, at the present time, realizing large additional improvements is difficult due to the backgrounds from $H \to b\bar{b}, c\bar{c}$ and $Zq\bar{q}$. However, if those backgrounds could be further suppressed, say by a factor 10, both single- and multi-angularity distributions could yield even better limits on y_q.

The paper is organized as follows: in section 2, we obtain the factorization of angularity distributions from Higgs boson decay in the formalism of SCET, allowing large logs in the distributions to be resummed through renormalization group evolution. Both the decay processes $H \to q\bar{q}$ and $H \to gg$ are calculated to NNLL + $\mathcal{O}(\alpha_s)$ accuracy. Although higher orders are now possible (e.g. [61]), for our illustrative study here, we do not include higher-order corrections. The numerical predictions are given in section 3. We then show the precision with which light quark Yukawa couplings could be measured using angularity distributions in section 4. Finally, we conclude in section 5. The one-loop angularity distributions in Higgs boson decay and some technical details of our analysis are discussed in the appendix.

2 Factorization and resummation of event shapes

2.1 Factorization of cross section in SCET

The angularities are defined as [59, 62],

$$\tau_a = \frac{1}{Q} \sum_i |p_T^i| e^{-|\eta_i|(1-a)}, \tag{2.1}$$

where, for us, we will take $Q = m_H = 125$ GeV, the sum is over all final state particles i. The pseudorapidity η_i and transverse momentum p_T^i of each particle i is measured with respect to the thrust axis [43, 63] in the rest frame of the Higgs boson. The parameter a defining each angularity τ_a is a continuous parameter $a < 2$ for infrared safety, though we will focus on $a < 0.5$ in this work, since soft recoil effects which complicate the resummation become important as $a \to 1$ [59, 64–68]. The angularities have found a wide range of applications in e^+e^- collisions producing hadrons (e.g. refs. [60, 69–73]), and their distributions have been calculated to NNLL′ resummed and $\mathcal{O}(\alpha_s^2)$ matched accuracy [60].

To describe the decay of Higgs boson, we will use the following effective Lagrangian,

$$\mathcal{L}_{\text{eff}} = \frac{\alpha_s(\mu)}{12\pi v} H G^{\mu\nu,b} G^b_{\mu\nu} + \sum_q \frac{y_q(\mu)}{\sqrt{2}} H \bar{\Psi}_q \Psi_q, \tag{2.2}$$

where μ is the renormalization scale, b is the color index (summed over) of the gluon field with field strength tensor $G^b_{\mu\nu}$. In our calculation, we ignore the masses of the light quarks, but keep the Yukawa coupling y_q itself. The coupling of the Higgs to the gluon fields comes from integrating out the top quark.

JHEP03(2024)123

For small values of $\tau_a \ll 1$, the degrees of freedom in the final state at leading power are collinear quarks and gluons in the two back-to-back directions in the Higgs rest frame, and (ultra)soft gluons radiated between them. We can predict the cross section in this regime by matching the operators in eq. (2.2) onto operators in SCET:

$$\bar{\Psi}_q \Psi_q \to C_2^q(m_H,\mu)\bar{\chi}_n\chi_{\bar{n}}, \quad G^{\mu\nu,b}G^b_{\mu\nu} \to C_2^g(m_H,\mu) m_H^2 g_{\mu\nu} B^{\mu,b}_{n\perp} B^{\nu,b}_{\bar{n}\perp}. \tag{2.3}$$

Here $\chi_{n,\bar{n}}$ and $B_{n\perp,\bar{n}\perp}$ are the SCET gauge invariant collinear quark and gluon fields respectively [74–77]. Computing the cross section in this regime, the event shape distributions in e^+e^- collisions can be factorized into hard, jet and soft functions [59, 60, 69, 70, 78],

$$\frac{d\Gamma^i_H}{\Gamma^i_{H0} d\tau_a} = H^i(m_H,\mu) \int d\tau_a^n d\tau_a^{\bar{n}} d\tau_a^s \delta\left(\tau_a - \frac{t_a^n + t_a^{\bar{n}}}{m_H^{2-a}} - \frac{k_s}{m_H}\right) J_n^i(t_a^n,\mu) J_{\bar{n}}^i(t_a^{\bar{n}},\mu) S^i(k_s,\mu), \tag{2.4}$$

where $i = q, g$ corresponds to $H \to q\bar{q}, gg$, $t_a^{n,\bar{n}}$ are the natural arguments of the jet functions of dimension $2-a$ [70, 78], and k_s is the natural dimension-1 argument of the soft function. The decay spectra in eq. (2.4) are normalized to the leading-order partial decay widths,

$$\Gamma^q_{H0} = \frac{y_q^2(m_H) m_H C_A}{16\pi}, \qquad \Gamma^g_{H0} = \frac{\alpha_s^2(m_H) m_H^3}{72\pi^3 v^2}. \tag{2.5}$$

$H^i(m_H,\mu)$ is the hard coefficient of Higgs boson decaying to quarks or gluons, and is given by the square of the matching coefficients in eq. (2.3),

$$H^i(m_H,\mu) = |C_2^i(m_H,\mu)|^2. \tag{2.6}$$

These encode virtual fluctuations at scales $\mu \sim m_H$ that give quantum corrections to the decay operators on the left-hand sides of eq. (2.3) that are integrated out of the lower-scale effective theory of collinear and soft excitations. At leading order in QCD factorization, soft wide-angle radiation can be shown to factor for the dynamics inside collinear jets [79], such that the sum of all soft emissions couple only to Wilson lines encoding the light-cone directions $n, \bar{n}$ of jets and their color representations. In SCET this is encapsulated in a field redefinition of collinear fields with soft Wilson lines so that soft gluons no longer couple directly to any collinear particles [77]. All collinear radiation and splitting inside jets are described by the jet functions, $J^i_{n,\bar{n}}(t_a^{n,\bar{n}},\mu)$, defined here by [71, 78]

$$\begin{aligned}
J_n^q(t_a^n,\mu) &= \frac{1}{2N_C} \int \frac{dl^+}{2\pi} \mathrm{Tr} \int d^4x\, e^{il\cdot x} \langle 0| \frac{\bar{\not{n}}}{2} \chi_n(x) \delta(t_a^n - Q^{2-a}\hat{\tau}_a^n) \delta(Q + \bar{n}\cdot\mathcal{P}) \delta^2(\mathcal{P}_\perp) \bar{\chi}_n(0) |0\rangle\,, \\
J_n^g(t_a^n,\mu) &= -\frac{Q}{2(N_C^2-1)} \int \frac{dl^+}{2\pi} \mathrm{Tr} \int d^4x\, e^{il\cdot x} \\
&\quad \times \langle 0| B^{\mu A}_{n\perp}(x) \delta(t_a^n - Q^{2-a}\hat{\tau}_a^n) \delta(Q - \bar{n}\cdot\mathcal{P}) \delta^2(\mathcal{P}_\perp) B^{\nu B}_{n\perp}(0) |0\rangle
\end{aligned} \tag{2.7}$$

where the traces are over color and Dirac (Lorentz) indices, the "label" momentum operators $\mathcal{P}^\mu$ fix the large label momentum components of the SCET collinear quark (gluon) fields χ_n ($B_{n\perp}$) [76] (here, $Q = m_H$), and $\hat{\tau}_a^n$ is an operator that fixes the angularity of final

JHEP03(2024)123

states produced by the collinear quark (gluon) fields [69]. Meanwhile, the soft functions $S^i(k^s,\mu)$ are defined by

$$S^q(k_s,\mu) = \frac{1}{N_C}\,\mathrm{Tr}\langle 0|\overline{T}[Y_{\bar n}Y_n^\dagger](0)\delta(k_s - Q\hat\tau_a^s)T[Y_nY_{\bar n}^\dagger](0)|0\rangle,$$
$$S^g(k_s,\mu) = \frac{1}{N_C^2-1}\,\mathrm{Tr}\langle 0|\overline{T}[\mathcal{Y}_{\bar n}\mathcal{Y}_n^\dagger](0)\delta(k_s - Q\hat\tau_a^s)T[\mathcal{Y}_n\mathcal{Y}_{\bar n}](0)|0\rangle, \tag{2.8}$$

where $Y_n(\mathcal{Y}_n)$ are soft Wilson lines in the fundamental (adjoint) representation along the direction of n_μ,

$$Y_n(x) = P\mathrm{exp}\left[ig_s\int_0^\infty ds\, n\cdot A_s(ns+x)\right], \tag{2.9}$$

with A_s in the fundamental representation, and $\mathcal{Y}_n$ is similar but in the adjoint representation.

In eqs. (2.7) and (2.8), the operators $\hat\tau_a^{n,s}$ acting on a collinear or soft final state returns the contribution to the angularity τ_a of that state, defined by its action on the collinear (soft) states $X_{n,s}$,

$$\hat\tau_a^{n,s}|X_{n,s}\rangle = \frac{1}{Q}\sum_{i\in X_{n,s}}|p_\perp^i|e^{-|\eta_i|(1-a)}|X_{n,s}\rangle\,, \tag{2.10}$$

and can also be constructed in terms of the energy-momentum tensor in QCD [69, 80–82].

In the next subsection we will review perturbative calculations of the above functions appearing in the factorized decay spectra and use them to evolve each piece and sum large logarithms in the full decay spectra.

2.2 RG evolution and resummation

The prediction for the decay spectrum eq. (2.4) in fixed order QCD perturbation theory contains logs of τ_a at every order in α_s, which become large for $\tau_a \ll 1$ and need to be resummed. This can be achieved by RG evolution of each piece of the factorized cross section (see, e.g. [78, 83]).

The Yukawa coupling $y_q(\mu)$ and strong coupling $\alpha_s(\mu)$ obey the following renormalization-group (RG) equations,

$$\mu\frac{d}{d\mu}y_q(\mu) = \gamma_y[\alpha_s(\mu)]y_q(\mu), \qquad \mu\frac{d}{d\mu}\alpha_s(\mu) = \beta[\alpha_s(\mu)]. \tag{2.11}$$

The anomalous dimension γ_y and the β function have expansions in α_s that we express:

$$\gamma_y[\alpha_s(\mu)] = \sum_{n=0}^\infty\left(\frac{\alpha_s}{4\pi}\right)^{n+1}\gamma_y^n, \qquad \beta[\alpha_s(\mu)] = -2\alpha_s\sum_{n=0}^\infty\left(\frac{\alpha_s}{4\pi}\right)^{n+1}\beta_n, \tag{2.12}$$

where the coefficients γ_y^n, β_n are given in eqs. (B.1) and (B.2). The one-loop hard functions are [84],

$$H^q(m_H,\mu) = 1 - \frac{\alpha_s(\mu)C_F}{2\pi}\left[\ln^2\frac{\mu^2}{m_H^2} + 3\ln\frac{\mu^2}{m_H^2} - 2 + \frac{7\pi^2}{6}\right],$$
$$H^g(m_H,\mu) = 1 - \frac{\alpha_s(\mu)}{2\pi}\left[C_A\ln^2\frac{\mu^2}{m_H^2} + \beta_0\ln\frac{\mu^2}{m_H^2} - \left(5+\frac{7\pi^2}{6}\right)C_A + 3C_F\right]. \tag{2.13}$$

JHEP03(2024)123

The soft functions for quark and gluon jets are known to one [85] and two loops [40, 86] for $a = 0$. For generic values of a, the soft function was computed to one loop order in [70]: the one-loop result in Laplace space is,

$$\widetilde{S}^i(\nu_a, \mu) = 1 - \frac{\alpha_s(\mu)}{4\pi} \frac{\pi^2}{1-a} C_i - \frac{\alpha_s(\mu)}{4\pi} \frac{8C_i}{1-a} \ln^2 \frac{\mu e^{\gamma_E} \nu_a}{m_H} \tag{2.14}$$

Here the color factor $C_i = C_{F,A}$ for quark and gluon respectively and ν_a is the Laplace-conjugate variable to the angularity τ_a. The two-loop soft functions for $a \neq 0$ have recently become computable using the program `SoftSERVE` [87–89], which were used for predictions of e^+e^- angularities to NNLL′ accuracy in [60]. To at least two-loop order, whether the directions of the $n, \bar{n}$ Wilson lines in eq. (2.8) are incoming or outgoing does not affect the perturbative results for the soft functions [90], so we can also use the results of [88, 89] here. We give the results for the non-cusp anomalous dimensions in eq. (B.5). The 2-loop constant terms for the quark channel can be found in [60, 89], though we will not use them in this paper, where we go only to NNLL+$\mathcal{O}(\alpha_s)$ accuracy.

The jet functions for massless quark and gluon jets are also known to one [91, 92], two [93, 94] and even three loops [95, 96] for $a = 0$. For generic values of a, the one-loop jet functions for quarks were computed in [70], and for gluons in [71, 97]. The result can be expressed in Laplace space,

$$\begin{aligned}\widetilde{J}^i(\nu_a, \mu) = 1 &+ \frac{\alpha_s(\mu)}{4\pi} \left[f_i(a) + \frac{2\pi^2 C_i}{3(1-a)(2-a)} \right] + \frac{\alpha_s(\mu)}{4\pi} \frac{4\gamma_i}{2-a} \ln \frac{\mu^{2-a} e^{\gamma_E} \nu_a}{m_H^{2-a}} \\ &+ \frac{\alpha_s(\mu)}{4\pi} \frac{4C_i}{(1-a)(2-a)} \ln^2 \frac{\mu^{2-a} e^{\gamma_E} \nu_a}{m_H^{2-a}},\end{aligned} \tag{2.15}$$

where the non-cusp anomalous dimension coefficient γ_i is given by,

$$\gamma_q = \frac{3}{2} C_F, \quad \gamma_g = \frac{\beta_0}{2}. \tag{2.16}$$

The coefficient of the constant term is a function of a, $f_i(a)$, which is defined as,

$$\begin{aligned} f_q(a) &= \frac{4C_F}{1-a/2} \left\{ \frac{7-13a/2}{4} - \frac{\pi^2}{12} \frac{3-5a+9a^2/4}{1-a} - \int_0^1 dx \frac{1-x+x^2/2}{x} \ln \left[(1-x)^{1-a} + x^{1-a} \right] \right\}, \\ f_g(a) &= \frac{2}{1-a/2} \left\{ C_A \left[(1-a) \left(\frac{67}{18} - \frac{\pi^2}{3} \right) - \frac{\pi^2}{6} \frac{(1-a/2)^2}{1-a} \right] - T_F n_f \frac{20-23a}{18} \right. \\ &\quad \left. - \int_0^1 dx \left[C_A \frac{(1-x+x^2)^2}{x(1-x)} + T_F n_f (1-2x+2x^2) \right] \ln \left[(1-x)^{1-a} + x^{1-a} \right] \right\} \end{aligned} \tag{2.17}$$

Here $T_F = \frac{1}{2}$, and $n_f = 5$ is the number of active quark flavors. The remaining integrals in the definitions of $f_{q,g}$ are easily evaluated numerically.

The hard, soft and jet functions $H, \widetilde{S}, \widetilde{J}$ obey the renormalization group equations (RGEs),

$$\mu \frac{d}{d\mu} F^i(\mu) = \gamma_F^i(\mu) F^i(\mu), \tag{2.18}$$

JHEP03(2024)123

where $F = H, \widetilde{S}, \widetilde{J}$. The anomalous dimension γ_F^i is given by,

$$\gamma_F^i(\mu) = -\kappa_F \Gamma^i_{\rm cusp}[\alpha_s] \ln \frac{\mu^{j_F} e^{\gamma_E} \nu_a}{m_H^{j_F}} + \gamma_F^i[\alpha_s]. \tag{2.19}$$

Here $\kappa_H = 4$, $\kappa_S = \frac{4}{2-a}$, $\kappa_J = -\frac{2}{1-a}$, $j_{H,S} = 1$ and $j_J = 2 - a$. Both the cusp and non-cusp anomalous dimensions can be expanded as,

$$\Gamma^i_{\rm cusp}[\alpha_s] = \sum_{n=0}^{\infty} \left(\frac{\alpha_s}{4\pi}\right)^{n+1} \Gamma^i_n, \qquad \gamma_F^i[\alpha_s] = \sum_{n=0}^{\infty} \left(\frac{\alpha_s}{4\pi}\right)^{n+1} \gamma^i_{Fn}. \tag{2.20}$$

The coefficients Γ^i_n and γ^i_{Fn} are given in appendix B.

For the two-loop jet functions for generic a, the cusp parts of the anomalous dimensions are known, while the non-cusp anomalous dimension for quark jets can be obtained from the hard and soft anomalous dimensions, by RG consistency,

$$\gamma_H + 2\gamma_J(a) + \gamma_S(a) = 0\,. \tag{2.21}$$

The two-loop constant terms for $a \neq 0$ for quark jets were obtained in [60] from numerical computations of the QCD singular cross section using EVENT2 [98, 99] together with the numerical results for soft function constants in [89]. Newer, highly precise results for $\gamma_J(a)$ and 2-loop constants for $a \neq 0$ for quark jet functions have been presented in [100]. Similar computations could be done for the gluon jet function for arbitrary a but lie outside the scope of this paper.

It is convenient to present the resummed results for the cumulative distribution,

$$\Gamma^i_{Hc} = \int_0^{\tau_a} d\tau'_a \frac{d\Gamma^i_H}{d\tau'_a}, \tag{2.22}$$

whose resummed form in momentum (τ_a) space is conveniently expressed in terms of the Laplace-transformed jet and soft functions acting with derivative operators on a resummation kernel [78, 101, 102]:

$$\begin{aligned}\frac{\Gamma^i_{Hc}}{\Gamma^i_{H0}} &= e^{\widetilde{K}^i(\mu_H,\mu_J,\mu_S,m_H)+K^i_\gamma(\mu_H,\mu_J,\mu_S)} \left(\frac{1}{\tau_a}\right)^{\Omega^i(\mu_J,\mu_S)} H^i(m_H,\mu_H) \\ &\quad \times \widetilde{J}^i\left(\partial_{\Omega^i} + \ln\frac{\mu_J^{2-a}}{m_H^{2-a}\tau_a}, \mu_J\right)^2 \widetilde{S}^i\left(\partial_{\Omega^i} + \ln\frac{\mu_S}{m_H\tau_a}, \mu_S\right) \frac{e^{\gamma_E\Omega^i}}{\Gamma(1-\Omega^i)}.\end{aligned} \tag{2.23}$$

Note that we use a form of the cusp evolution kernel proposed in [60] that keeps the resummed cross section explicitly independent of the factorization scale μ appearing in the original factorized cross section eq. (2.4), at every order in resummed perturbation theory,

$$\widetilde{K}^i_\Gamma(\mu,\mu_F,Q) = \int_{\mu_F}^{\mu} \frac{d\mu'}{\mu'} \Gamma^i_{\rm cusp}[\alpha_s(\mu')] \ln\frac{\mu'}{Q}. \tag{2.24}$$

While the other evolution kernels are defined as follows,

$$\eta^i_\Gamma(\mu,\mu_F) = \int_{\mu_F}^{\mu} \frac{d\mu'}{\mu'} \Gamma^i_{\rm cusp}[\alpha_s(\mu')], \qquad K^i_{\gamma_F}(\mu,\mu_F) = \int_{\mu_F}^{\mu} \frac{d\mu'}{\mu'} \gamma^i_F[\alpha_s(\mu')]. \tag{2.25}$$

JHEP03(2024)123

Explicit expansions order by order for these kernels are given in [60]. The sums of individual hard, jet, and soft evolution kernels Ω^i, $\widetilde{K}^i$ and K^i_γ used in eq. (2.23) are defined,

$$\begin{aligned}
\Omega^i \equiv \Omega^i(\mu_J, \mu_S) &= -2\kappa_J \eta^i_\Gamma(\mu, \mu_J) - \kappa_S \eta^i_\Gamma(\mu, \mu_S), \\
K^i_\gamma(\mu_H, \mu_J, \mu_S) &\equiv K^i_{\gamma_H}(\mu, \mu_H) + 2K^i_{\gamma_J}(\mu, \mu_J) + K^i_{\gamma_S}(\mu, \mu_S), \\
\widetilde{K}^i(\mu_H, \mu_J, \mu_S, Q) &\equiv -4\widetilde{K}^i_\Gamma(\mu, \mu_H, Q) - 2j_J\kappa_J \widetilde{K}^i_\Gamma(\mu, \mu_J, Q) - \kappa_S \widetilde{K}^i_\Gamma(\mu, \mu_S, Q).
\end{aligned} \tag{2.26}$$

2.3 Fixed-order matching

In order to obtain a reliable prediction for large values of τ_a, we also need to match our calculation to the full QCD fixed-order distribution. To $\mathcal{O}(\alpha_s)$, the full QCD distribution is,

$$\frac{1}{\Gamma^i_{H0}} \frac{d\Gamma^i_H}{d\tau_a}\bigg|_{\text{QCD}} = \delta(\tau_a) + \left(\frac{\alpha_s}{2\pi}\right) A^i_a(\tau_a) + \mathcal{O}(\alpha_s^2). \tag{2.27}$$

We follow the method in ref. [70] to calculate the coefficient $A^i_a(\tau_a)$ numerically. The detail of the calculation can be found in the appendix. Analytical results are only known for $a = 0$, found, e.g. in refs. [37, 55, 103].

The fixed-order angularity in SCET at $\mathcal{O}(\alpha_s)$ is given by,

$$\frac{1}{\Gamma^i_{H0}} \frac{d\Gamma^i_H}{d\tau_a}\bigg|_{\text{SCET}} = \delta(\tau_a) D^{\delta i}_a + \left(\frac{\alpha_s}{2\pi}\right) [D^i_a(\tau_a)]_+. \tag{2.28}$$

For quark final state,

$$\begin{aligned}
D^{\delta q}_a &= 1 - \frac{\alpha_s}{2\pi}\frac{C_F}{2-a}\bigg\{2 + 5a - \frac{\pi^2}{3}(2+a) + 6(a-2) \\
&\qquad + 4\int_0^1 dx \frac{x^2 - 2x + 2}{x} \ln\left[x^{1-a} + (1-x)^{1-a}\right]\bigg\}, \\
D^q_a(\tau_a) &= -\frac{2C_F}{2-a}\frac{\theta(\tau_a)(3 + 4\ln\tau_a)}{\tau_a}.
\end{aligned} \tag{2.29}$$

For gluon final state,

$$\begin{aligned}
D^{\delta g}_a &= 1 + \frac{\alpha_s}{2\pi}\left\{\left(5 + \frac{7\pi^2}{6}\right) C_A - 3C_F + \frac{C_A}{1-a}\frac{\pi^2}{6} + 2f_g(a)\right\}, \\
D^g_a(\tau_a) &= -\frac{2}{2-a}\frac{\theta(\tau_a)\,(\beta_0 + 4C_A \ln\tau_a)}{\tau_a},
\end{aligned} \tag{2.30}$$

where the function f_g was given in eq. (2.17). We define the difference away from $\tau_a = 0$ between full QCD and SCET as,

$$r^i_a(\tau_a) = A^i_a(\tau_a) - D^i_a(\tau_a). \tag{2.31}$$

Note that the coefficient $\alpha_s/(2\pi)$ is not included in the above definition. We need to add this remainder function to the resummed distribution in order to obtain the NLL$' + \mathcal{O}(\alpha_s)$ and NNLL $+ \mathcal{O}(\alpha_s)$ accuracy. The numerical results of $r^i_a(\tau_a)$ for values of a equal to $\{-1.0, -0.5, 0.0, 0.25, 0.5\}$ are shown in figure 1. The kink in figure 1 at $\tau_a^{\max} = \frac{1}{3^{1-a/2}}$ is

JHEP03(2024)123

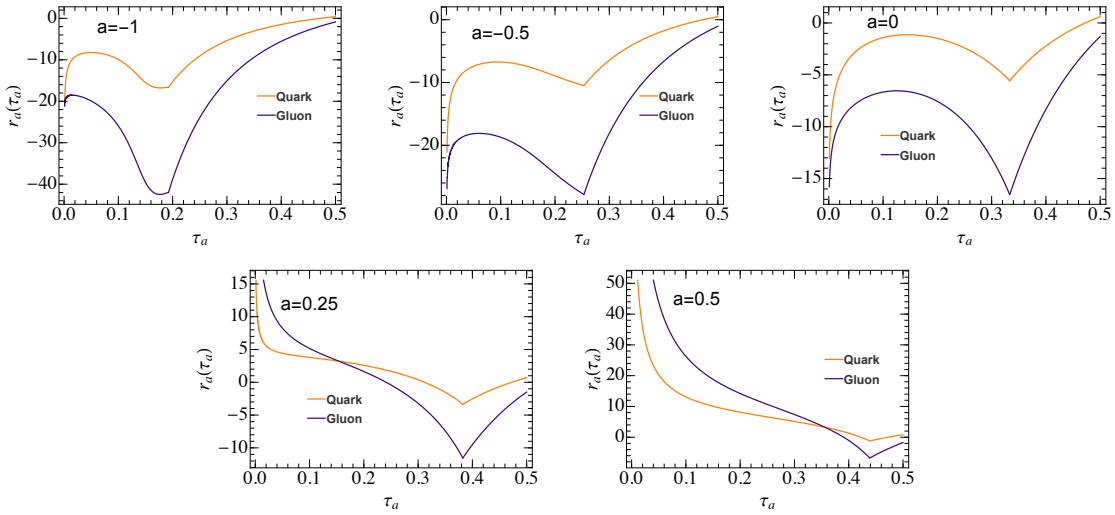

Figure 1. The $\mathcal{O}(\alpha_s)$ nonsingular remainder functions for Higgs decaying to quarks (orange) and gluons (purple). Their relative size compared to the singular and total fixed-order cross sections is shown in figure 2.

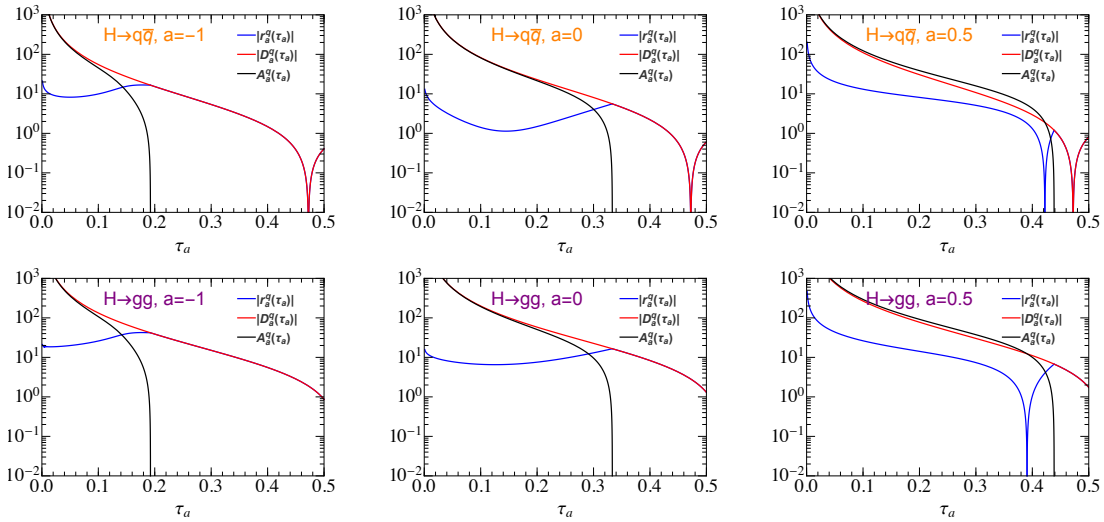

Figure 2. The singular and nonsingular distributions for $a = (-1.0, 0.0, 0.5)$. The value of τ_a where the singular (black) and nonsingular (blue) cross determines the transition point $\tau_a = t_2(a)$ between resummation and fixed-order regions that will be used in the scale profile functions later.

due to the fact that the full QCD distribution vanishes above the maximum kinematic value of τ_a and only the singular part will give a contribution above this value. As an important consistency check of this matching technique, we integrate over τ_a to get the fixed-order correction for the Higgs partial decay width. The total partial decay width can be written as,

$$\Gamma^i_{\text{Htot}} = \Gamma^i_{H0}\left(1 + \frac{\alpha_s(m_H)}{2\pi}\Gamma^i_{H1}\right). \tag{2.32}$$

The numerical results of Γ^i_{H1} are summarized in table 1. It shows our results are in agreement with ref. [104] for all the values of a of we are interested in.

JHEP03(2024)123

a	-1.0	-0.5	0.0	0.25	0.5	NLO [104]
Γ^q_{H1}	11.33	11.33	11.33	11.33	11.30	11.34
Γ^g_{H1}	35.83	35.83	35.83	35.83	35.77	35.83

Table 1. NLO QCD correction for the Higgs partial decay width for selected values of a.

2.4 Nonperturbative shape function

The soft function in the factorization theorem will also receive corrections from nonperturbative hadronization effects. It can be parameterized into a soft shape function $f_{\rm mod}(k)$ as [105–107],

$$S^i(k,\mu) = \int dk' S^i_{\rm PT}(k-k',\mu) f^i_{\rm mod}(k'-2\bar{\Delta}^i_a). \tag{2.33}$$

Here $S^i_{\rm PT}$ is the perturbative soft function and $\bar{\Delta}^i_a = \frac{\bar{\Delta}^i}{1-a}$ is a gap parameter with $\bar{\Delta}^i \sim \Lambda_{\rm QCD}$ and $\bar{\Delta}^i$ is an a-independent parameter. This scaling of $\bar{\Delta}^i_a$ tracks the known scaling $1/(1-a)$ of the first moment of the shape function [62, 108]. The shape function can be expanded in a complete set of orthonormal basis functions [109],

$$f^i_{\rm mod}(k) = \frac{1}{\lambda_i}\left[\sum_{n=0}^{\infty} b_n f_n\left(\frac{k}{\lambda_i}\right)\right]^2, \tag{2.34}$$

where

$$f_n(x) = 8\sqrt{\frac{2x^3(2n+1)}{3}} e^{-2x} P_n(g(x)), \qquad g(x) = \frac{2}{3}\left[3 - e^{-4x}\left(3+12x+24x^2+32x^3\right)\right] - 1. \tag{2.35}$$

Here P_n are Legendre polynomials. In our calculation, we will only keep $b_0 = 1$ and set $b_n = 0$ for $n > 0$. The parameter λ_i corresponds to the first moment of the $f_{\rm mod}$. However, it has been shown in ref. [107] that the gap parameter $\bar{\Delta}_a$ has a renormalon ambiguity. To ensure good perturbative convergence of the soft function eq. (2.33) and resulting cross section, as well as a stable definition of $\bar{\Delta}^i_a$, it is necessary to subtract/add a series removing this ambiguity from both $S_{\rm PT}$ and $\bar{\Delta}^i_a$. In order to cancel the ambiguity, we can split the gap parameter as,

$$\bar{\Delta}^i_a = \Delta^i_a(\mu_S, R) + \delta^i_a(\mu_S, R), \tag{2.36}$$

where δ^i_a can be perturbative expansion with a same renormalon ambiguity as $S^i_{\rm PT}$ and Δ^i_a is a renormalon free parameter. The R is the subtraction scale, which is defined through,

$$Re^{\gamma_E}\frac{d}{d\ln\nu}\left[\ln\left(e^{-2\nu\delta^i_a(\mu)}\widetilde{S}^i_{\rm PT}(\nu,\mu)\right)\right]_{\nu=1/(Re^{\gamma_E})} = 0, \tag{2.37}$$

where $\nu = \nu_a/m_H$, the same scheme adopted in, e.g. [39, 60, 110]. There are multiple other schemes to define the series δ^i_a, see e.g. [111], and one could study the quantitative effects of varying schemes (cf. [112]), though this lies outside the scope of this paper. The shift eq. (2.36) results in the renormalon-free soft function,

$$S^i(k,\mu) = \int dk' S^i_{\rm PT}(k-k'-2\delta^i_a(\mu,R),\mu) f^i_{\rm mod}(k'-2\Delta^i_a). \tag{2.38}$$

JHEP03(2024)123

The non-perturbative effects will shift the perturbative cross section. The shift parameter $\overline{\Omega}^i(\mu, R)$ is given by,

$$\frac{2\overline{\Omega}^i(\mu, R)}{1-a} = 2\Delta_a^i(\mu, R) + \int dk\, k f^i_{\rm mod}(k). \tag{2.39}$$

In our calculation, we choose $\overline{\Omega}^q(R_\Delta, R_\Delta) = 0.4$ GeV and $\Delta_a^i(R_\Delta, R_\Delta) = \frac{0.1\text{ GeV}}{1-a}$ with the reference scale $R_\Delta = 1.5$ GeV. We also assume the Casimir scaling for the parameter $\overline{\Omega}^g(R_\Delta, R_\Delta) = \overline{\Omega}^q(R_\Delta, R_\Delta)C_A/C_F$. This is purely an assumption, though probably fairly good, that we make to simplify our illustrative analysis below. A definitive study should measure $\overline{\Omega}^{q,g}$ separately. The gap parameter Δ_a^i can be evolved to any other subtraction scale R and soft scale μ_S, using the formalism in [113, 114], formulas also summarized in ref. [60].

2.5 Scales in resummation

From the arguments of the logarithms in the hard, jet and soft functions, the canonical scales should be,

$$\mu_H = m_H, \qquad \mu_J = m_H \tau_a^{1/(2-a)}, \qquad \mu_S = m_H \tau_a. \tag{2.40}$$

However, the canonical scales do not properly take into account the transition from the resummation region into the fixed-order region where τ_a is not small or into the nonperturbative region for $\tau_a \leq \Lambda_{\rm QCD}/m_H$. The use of profile scales has been proposed to smooth the transition between those different scale regions [39, 109] and various specific forms for these profile functions are possible, e.g. [39, 60, 97, 115]. We use:

$$\begin{aligned}
\mu_H &= e_H m_H, \\
\mu_S(\tau_a) &= \left[1 + e_S \theta(t_3 - \tau_a)\left(1 - \frac{\tau_a}{t_3}\right)^2\right] \mu_{\rm run}(\tau_a), \\
\mu_J(\tau_a) &= \left[1 + e_J \theta(t_3 - \tau_a)\left(1 - \frac{\tau_a}{t_3}\right)^2\right] \mu_H^{\frac{1-a}{2-a}} \mu_{\rm run}(\tau_a)^{\frac{1}{2-a}},
\end{aligned} \tag{2.41}$$

where e_H simply controls the normalization of the hard scale, while $e_{J,S}$ control variations of the shape of the jet and soft scales as a function of τ_a above and below their default, canonical shapes. The ranges over which we vary them are given in table 2. (Actually we keep $e_S = 0$ as variations of other parameters below will make varying e_S redundant.) The running scale is defined as,

$$\mu_{\rm run} = \begin{cases}
\mu_0, & \tau_a \leq \tau_0, \\
\zeta\left(\tau_a; \{t_0, \mu_0, 0\}, \{t_1, 0, \frac{r}{\tau_a^{\rm sph}\mu_H}\}\right), & t_0 \leq \tau_a \leq t_1, \\
\frac{r}{\tau_a^{\rm sph}}\mu_H \tau_a, & t_1 \leq \tau_a \leq t_2, \\
\zeta\left(\tau_a; \{t_2, 0, \frac{r}{\tau_a^{\rm sph}\mu_H}\}, \{t_3, \mu_H, 0\}\right), & t_2 \leq \tau_a \leq t_3, \\
\mu_H, & \tau_a \geq t_3.
\end{cases} \tag{2.42}$$

The function ζ smoothly transitions between regions, and is defined as

$$\zeta\left(\tau_a; \{t_0, y_0, r_0\}, \{t_1, y_1, r_1\}\right) = \begin{cases}
a + r_0(\tau_a - t_0) + c(\tau_a - t_0)^2, & \tau_a \leq \frac{\tau_0+\tau_1}{2} \\
A + r_1(\tau_a - t_1) + C(\tau_a - t_1)^2, & \tau_a \geq \frac{\tau_0+\tau_1}{2}
\end{cases}, \tag{2.43}$$

JHEP03(2024)123

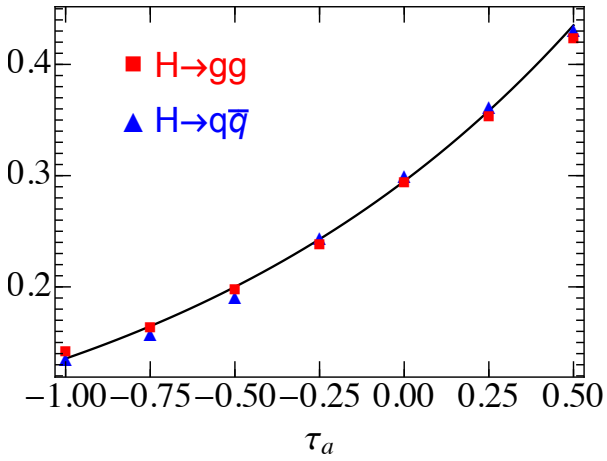

Figure 3. The value of $t_2(a)$ with $a = (-1.0, -0.75, -0.5, -0.25, 0.0, 0.25, 0.5)$, determined by the crossing of singular and nonsingular parts of the cross section in figure 2. The blue triangle is from $H \to q\bar{q}$, while the red box is for $H \to gg$. The black line is the fitting function $t_2 = 0.295^{1-0.637a}$.

where the coefficients are

$$a = y_0 + r_0 t_0, \quad A = y_1 + r_1 t_1, \quad c = 2\frac{A-a}{(t_0-t_1)^2} + \frac{3r_0+r_1}{2(t_0-t_1)}, \quad C = 2\frac{a-A}{(t_0-t_1)^2} + \frac{3r_1+r_0}{2(t_1-t_0)}. \tag{2.44}$$

The parameters t_i are used to control the transition of different regions and we parameterized them as,

$$t_0 = \frac{n_0}{m_H} 3^a, \qquad t_1 = \frac{n_1}{m_H} 3^a, \qquad t_2 = n_2 \times 0.295^{1-0.637a}, \qquad t_3 = n_3 \tau_a^{\rm sph}. \tag{2.45}$$

Here $\tau_a^{\rm sph} = \frac{1}{2-\frac{a}{2}}\ {}_2F_1\left(1, -\frac{a}{2}; 3-\frac{a}{2}; -1\right)$ is the angularity of the spherically symmetric configuration. The parameters t_0 and t_1 control the transition between the non-perturbative and resummation regions. In the nonperturbative region, we freeze the scale at $\mu_{\rm run} \sim 1 - 3\,\text{GeV}$ to allow the a shape function to smoothly describe this region and avoid the Landau pole in $\alpha_s(\mu)$. The parameter t_2 was determined by the point where singular and nonsingular contribution become comparable. As an example, we show the value of t_2 for $a = (-1.0, 0.0, 0.5)$ in figure 2, and it is determined by the crossing points of blue and black lines. It shows the t_2 is almost same for $H \to q\bar{q}$ and $H \to gg$, see figure 3. The particular functional form in eq. (2.45) is the same as that found for 1-jettiness in DIS in [115], and the same form happens to fit the transition points plotted in figure 3 as well. Therefore, we will use the same t_2 formula for both Higgs decaying to quark and gluon states. Now, the exact values of $t_{0,1,2,3}$ are somewhat arbitrary, thus we vary them using the parameters $n_{0,1,2,3}$ to estimate theoretical uncertainties, across ranges given in table 2.

For the renormalon subtraction scale, we choose $R(\tau_a) = \mu_S(\tau_a)$ with $\mu_0 \to R_0$ and initial value of $R_0 < \mu_0$ for $\tau_a < t_0$. The remainder function depends on another scale $\mu_{\rm ns}$ which

JHEP03(2024)123

e_H	e_J	e_S	$n_0(q)$	$n_0(g)$
$0.5 \leftrightarrow 2$	$-0.5 \leftrightarrow 0.5$	0	$1 \leftrightarrow 2$ GeV	$2.8 \leftrightarrow 3.5$ GeV
$n_1(q)$	$n_1(g)$	n_2	n_3	$\mu_0(q)$
$8.5 \leftrightarrow 11.5$ GeV	$25 \leftrightarrow 28$ GeV	$0.9 \leftrightarrow 1.1$	$0.8 \leftrightarrow 0.9$	$1.0 \leftrightarrow 1.2$ GeV
$\mu_0(g)$	$R_0(q)$	$R_0(g)$	r	
$2.2 \leftrightarrow 3.0$ GeV	$\mu_0(q) - 0.4$ GeV	$\mu_0(g) - 1.8$ GeV	$0.75 \leftrightarrow 1.33$	

Table 2. The parameter ranges for our theoretical uncertainty estimation [60]. Note that we use the different parameters $n_{0,1}$, μ_0 and R_0 for quark and gluon final states.

is used to estimate the higher-order effects from fixed order calculation [41],

$$\mu_{\rm ns}(\tau_a) = \begin{cases} \frac{1}{2}(\mu_H + \mu_J(\tau_a)), & n_s = 1 \\ \mu_H, & n_s = 0 \\ \frac{1}{2}(3\mu_H - \mu_J(\tau_a)), & n_s = -1 \end{cases} .$$

The values we pick for R_0 for quark and gluon τ_a distributions are also given in table 2.

3 Numerical results

Below, we present the numerical results of angularity distributions from Higgs boson decaying to quarks and gluons at NLL$' + \mathcal{O}(\alpha_s)$ and NNLL $+ \mathcal{O}(\alpha_s)$ accuracy. In order to obtain a comprehensive theory uncertainty, we should consider all the scales and parameters from the profile function in our calculation. For a conservative estimation, we use the scan method to calculate the uncertainty band [39], and take 64 random selections of profile and scale parameters within the ranges shown in table 2. Note that the soft scale parameter e_S has been fixed to zero and the variation of soft scale μ_S is from other parameters, e.g. n_0, n_1, μ_0, r. In figure 4, we show the integrated distribution $\Gamma^i_{Hc}(\tau_a)$ for five values of angularity parameter $a = (-1.0, -0.5, 0.0, 0.25, 0.5)$ to NLL$' + \mathcal{O}(\alpha_s)$ and NNLL $+ \mathcal{O}(\alpha_s)$ accuracy. Note that the total partial decay width $\Gamma^i_{\rm Htot}$ is defined with the renormalization scale $\mu = m_H$. From NLL$' + \mathcal{O}(\alpha_s)$ to NNLL $+ \mathcal{O}(\alpha_s)$, the scale uncertainties can reduce a little and the correction is sizable for small a, e.g. $a = -1$. It is also clear that the quark and gluon decay modes from Higgs boson show different shapes in the small τ_a region since the different color structure of quark and gluon. Therefore, the precise study of the angularity event shapes offers the possibility to distinguish the quark and gluon jets from Higgs boson decay and further can be used to constrain the light quark Yukawa couplings.

The differential distribution of angularities can be obtained by taking the derivative of eq. (2.23); see figure 5 for the numerical results. We note that the gluon distributions peak at much larger values compared to the quark case. It could be understood from the Casimir scaling C_A/C_F in Sudakov factor. The distributions from gluon are also much broader compared to the quark cases due to the stronger QCD radiation. We also find that the larger a would shift the peak to a larger value. This is because varying a will change the proportions of two-jet-like events and three-or-more-jet-like events and further to change the peak position of the τ_a distributions.

JHEP03(2024)123

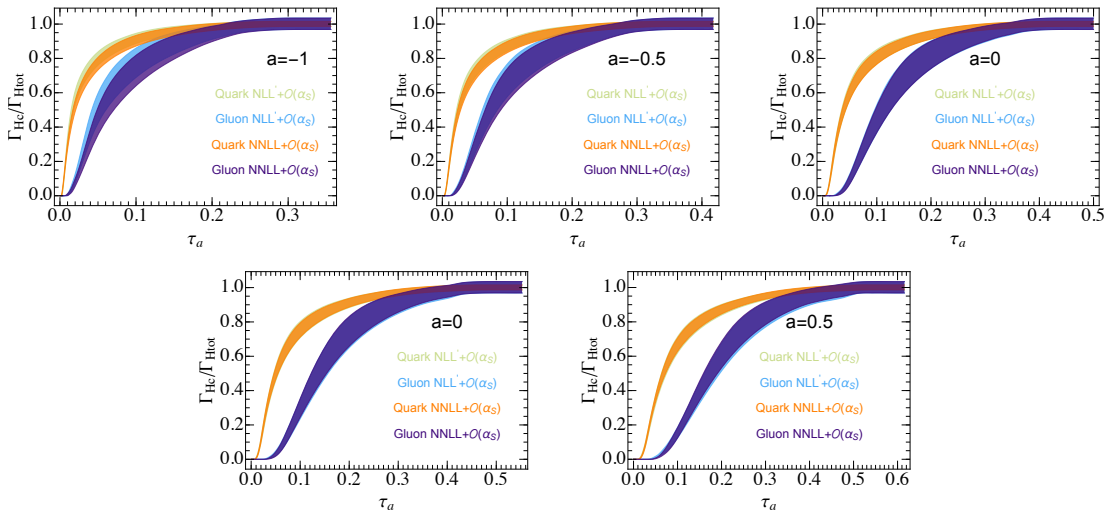

Figure 4. Integrated angularity distributions for values of $a = (-1.0, -0.5, 0.0, 0.25, 0.5)$ at NLL$'$ + $\mathcal{O}(\alpha_s)$ (green for quark and blue for gluon) and NNLL + $\mathcal{O}(\alpha_s)$ (orange for quark and purple for gluon), including shape function effects. The theoretical uncertainties have been estimated with the scan method.

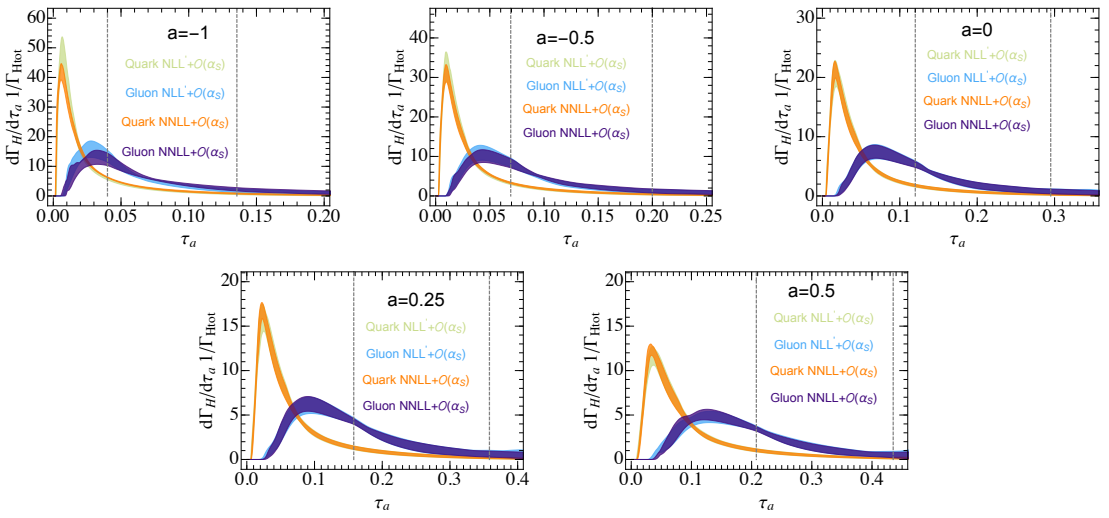

Figure 5. Differential angularity distributions for values of $a = (-1.0, -0.5, 0.0, 0.25, 0.5)$ at NLL$'$ + $\mathcal{O}(\alpha_s)$ (green for quark and blue for gluon) and NNLL + $\mathcal{O}(\alpha_s)$ (orange for quark and purple for gluon) for Higgs decay, including shape function effects. The theoretical uncertainties have been estimated with the scan method. The perpendicular dashed lines denote the analysis regions $[\tau_{\min}(a), \tau_{\max}(a)]$ for probing light quark Yukawa couplings.

JHEP03(2024)123

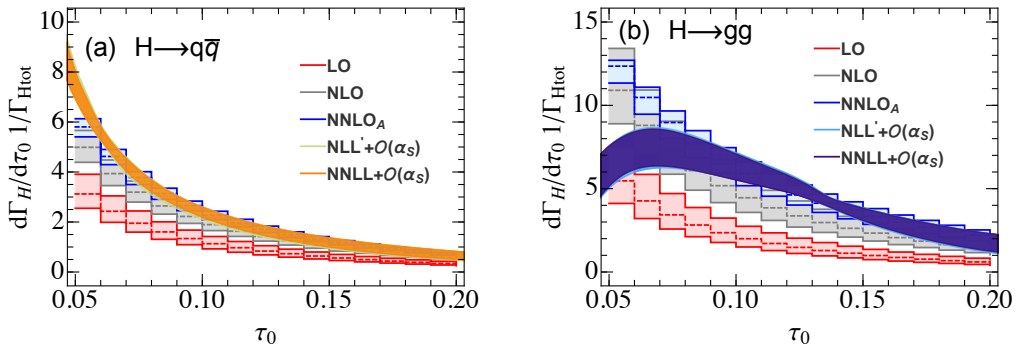

Figure 6. The normalized thrust distributions for Higgs decaying to quark and gluons at NLL′ + $\mathcal{O}(\alpha_s)$ and NNLL + $\mathcal{O}(\alpha_s)$ accuracy (green and orange for $H \to q\bar{q}$ and light blue and purple for $H \to gg$), including a nonperturbative shape function, compared to LO (red), NLO (gray) and approximate NNLO (blue). The fixed order prediction is from [55]. Note that the normalization factor $\Gamma_{\rm Htot}$ is defined in NLO.

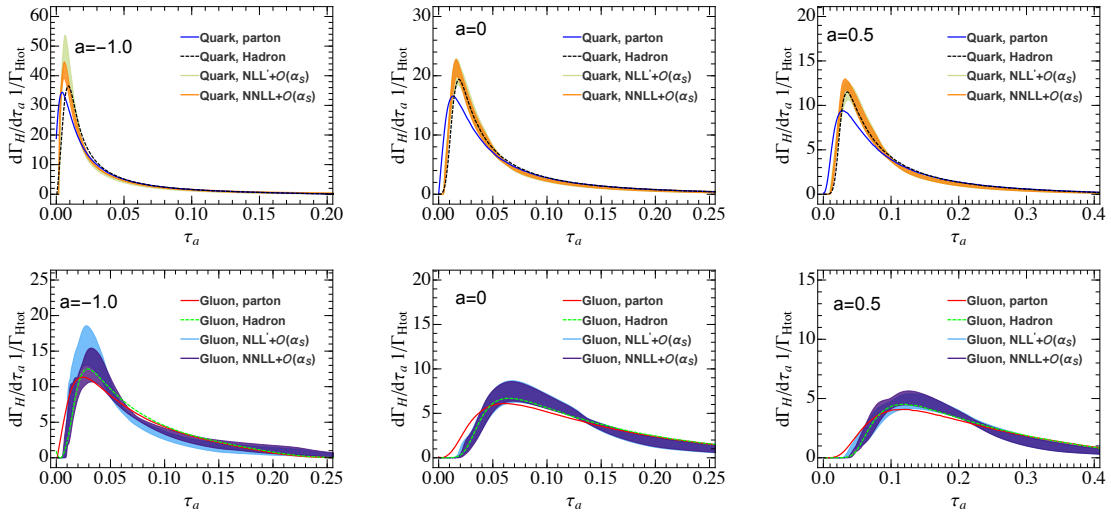

Figure 7. The normalized angularity distributions for Higgs decaying to quark and gluons at NLL′ + $\mathcal{O}(\alpha_s)$ and NNLL + $\mathcal{O}(\alpha_s)$ accuracy, including shape function effects, compared to PYTHIA at parton level (solid lines) and hadron level (dashed lines) for $a = (-1.0, 0, 0.5)$.

In figure 7, we compare our theoretical calculation of Higgs decaying to quarks and gluons to PYTHIA [116] at parton and hadron levels. It shows that PYTHIA predictions at hadron level agree with our theoretical calculation very well, but the parton level results do not in the nonperturbative region at very small τ_a. We should note that the design of profile functions is somewhat of an art. The choices of the parameters are based on obtaining properties of the theoretical predictions such as smoothness and convergence of uncertainty bands.

Since the thrust from Higgs boson decay has been calculated up to approximate NNLO (i.e. full NLO and singular NNLO) accuracy, it is also useful to compare our resummed results with the fixed order prediction in ref. [55]; see figure 6. It shows that our resummed prediction (which includes a shape function) agrees with the NNLO prediction very well

JHEP03(2024)123

in Higgs decaying to quark or gluon states at sufficiently large τ_0, but there are deviations in the small τ_0 region, where especially for gluons, where the effects of resummation and of the nonperturbative shape function cause the distribution to peak at some value of τ_0. However, if we focus on the region $\tau_0 \in [0.1, 0.20]$, our results agree with the approximate NNLO very well for both quark and gluon final states.

Our theoretical predictions show in figures 4–7 include a soft shape function eq. (2.38), with parameters chosen simply as described there. No attempt has been made to tune this for Higgs decay, they were guided simply by similar values they take in event shapes in $e^+e^- \to$ hadrons (e.g. [39, 41]), for purposes of producing illustrative numerical predictions. When a serious comparison to data is performed, the data can be used to constrain these soft shape function model parameters and test properties such as the universal scaling properties of the leading nonperturbative shift governed by $\Omega_1^{q,g}$ [62, 108].

4 Probing light quark Yukawa couplings

Next, we will use angularity distributions to probe light quark Yukawa couplings at CEPC and our results are easy to generalize to other e^+e^- colliders. At CEPC, the Higgs boson is dominantly produced through the Higgs and Z boson associated production, i.e. $e^+e^- \to HZ$. The signal we are interested in is Higgs decaying into $q\bar{q}$ with $q = u, d, s$ and Z boson decaying into lepton pairs. The major SM backgrounds are $H(\to gg, b\bar{b}, c\bar{c})Z$, $Zq\bar{q}$ and $H(\to VV^* \to 4j)Z$, with $V = W^\pm, Z$.[1] To suppress the backgrounds from heavy quarks, we could use flavor tagging techniques. Ref. [42] has shown in this case that the heavy flavor backgrounds can be removed mostly if we require two non-b and c jets in the final state. The background $Zq\bar{q}$ can be highly suppressed after we include the kinematical cuts, e.g. recoil mass [22, 117]. As shown in ref. [42], after the kinematical cuts and requiring two light jets in the final state, we could get the number of background events for the $H \to gg$ down to $N_b^g = 3070$ at $\sqrt{s} = 250$ GeV with an integrated luminosity of 5 ab^{-1}. The background of Higgs decaying to heavy flavor quarks ($H \to b\bar{b}, c\bar{c}$) is about $N_b^{\rm HF} = 0.1N_b^g$, and the number of $Zq\bar{q}$ events is $N_b^{\rm ZZ} = 0.2N_b^g$. The background of $H \to VV^*$ will contribute to the tail region of the angularity distributions and the number of events after including above analysis is $N_b^{\rm 4q} = 0.6\ N_b^g$ [42]. It is clear that the gluon background is the major obstacle for probing light quark Yukawa couplings. Therefore, we propose to use the hadronic angularity distributions of Higgs boson to separate the gluon background from the signal. We should note that the kinematical cuts in this section just modify the normalization but not the shape of the τ_a distributions. Thus, we could use the normalized angularity distributions to study the Yukawa couplings without input any kinematical cuts for the signal and backgrounds.

In this work, we assume NP effects only change the branching ratio (BR) of Higgs decaying to light quarks, then we define the ratio,

$$R_q = \frac{\mathrm{BR}(H \to q\bar{q})}{\mathrm{BR}(H \to gg)} = \frac{9C_A\pi^2 v^2}{2m_H^2} \frac{y_q^2(m_H)}{\alpha_s^2(m_H)} \frac{1 + \alpha_s(m_H)/(2\pi)\Gamma_{H1}^q}{1 + \alpha_s(m_H)/(2\pi)\Gamma_{H1}^g}. \tag{4.1}$$

[1] In case one is concerned about an additional Zgg final state background, since it can only be generated by $ZH(H \to gg)$ production, it is precisely the one we are trying to suppress by measuring τ_a on the final state.

JHEP03(2024)123

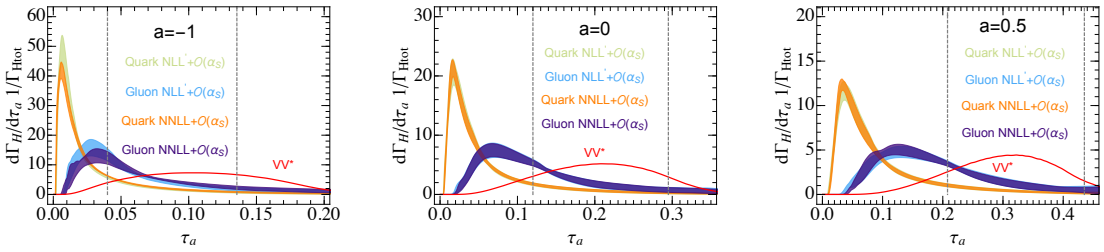

Figure 8. The normalized distributions of angularity from PYTHIA at hadron level for $H \to VV^* \to 4j$ with $a = (-1.0, 0.0, 0.5)$ (red lines). The orange and purple lines are from our theoretical prediction for $H \to q\bar{q}$ and $H \to gg$. The perpendicular dashed lines denote the analysis regions $[\tau_{\min}(a), \tau_{\max}(a)]$ for probing light quark Yukawa couplings.

The 1-loop corrections $\Gamma_{H1}^{q,g}$ to the Higgs decay widths were given in eq. (2.32) and table 1. The total number of signal events is $N_s = R_q N_b^g$.

In the SM, $R_q \simeq 0$ due to the smallness of the quark mass. We divide the angularity into $N_{\rm bin} = 10$ bins and use the binned likelihood function to estimate the sensitivity for the hypothesis with R_q against the hypothesis with $R_q = 0$ [118],

$$L(R_q) = \prod_{i=1}^{N_{\rm bin}} \frac{(s_i(R_q) + b_i)^{n_i}}{n_i!} e^{-s_i(R_q)-b_i}, \tag{4.2}$$

where b_i and n_i are the number of the backgrounds and observed event in the ith bin, respectively, and $s_i(R_q)$ is the number of signal events in the ith bin for the parameter R_q. We set $n_i = s_i(0) + b_i$. The number of signal events in each bin is determined by our theoretical calculation at NNLL + $\mathcal{O}(\alpha_s)$ accuracy. The number signal events in the ith bin is,

$$s_i(R_q) = N_s \int_i d\tau_a \frac{1}{\Gamma_{Htot}^q} \frac{d\Gamma_H^q}{d\tau_a}, \tag{4.3}$$

The normalized angularity distributions from $H \to b\bar{b}, c\bar{c}$ are almost same with $H \to q\bar{q}$ except for very small τ_a region due to the mass effect of heavy quark. In order to avoid the possible heavy quark mass effect, the impact of non-perturbative function and the contamination of high tail backgrounds, we can very conservatively require $\tau_{\min}(a) < \tau_a < \tau_{\max}(a)$ with $\tau_{\min}(a) = \frac{15}{125} \times 3^a$ and $\tau_{\max}(a) = 0.295^{1-0.637a}$ (see the vertical dashed lines in figure 5). Therefore, we expect the angularity distributions from heavy quarks should be same with the light quarks in this region. The distributions from $Zq\bar{q}$ should have the same shape as those predicted in ref. [60] at NNLL$'$ + $\mathcal{O}(\alpha_s^2)$ accuracy. The background $H \to VV^*$ can be estimated by event generator Madgraph [119] and PYTHIA [116] at the leading order; see figure 8. It is clear that the four-quark background from gauge boson pair is only sensitive to the tail region and far away from the peak of the signal. The total backgrounds in ith bin is,

$$b_i = \sum_j N_b^j \int_i d\tau_a \frac{1}{\Gamma_{Htot}^j} \frac{d\Gamma_H^j}{d\tau_a}. \tag{4.4}$$

Here $j = g, \mathrm{HF}, \mathrm{ZZ}, 4\mathrm{q}$ denotes the different background processes.

JHEP03(2024)123

We define the test ratio of likelihood function,

$$q^2 = -2 \ln \frac{L(R_q)}{L(0)}. \tag{4.5}$$

The parameter q yields the exclusion of the hypothesis 1 with $R_q \neq 0$ versus the hypothesis 0 with $R_q = 0$ at the $q\sigma$ confidence level. Thus,

$$q^2 = 2 \left[\sum_{i=1}^{N_{\rm bin}} n_i \ln \frac{n_i}{n_i(R_q)} + n_i(R_q) - n_i \right], \tag{4.6}$$

where $n_i(R_q) = s_i(R_q) + b_i$. For simplicity, we normalize the light quark Yukawa couplings to the SM bottom quark $y_b \equiv y_b(m_H)$. Figure 9 displays the expected 1σ (green) and 2σ (orange) confidence level exclusion limit on Yukawa coupling $y_q \equiv y_q(m_H)$ from the angularity distributions. It shows that the angularity event shapes, in the conservative τ_a window we considered above, could give a fairly strong constraint for the light quark Yukawa couplings, i.e. $y_q \lesssim 0.15 y_b$ (for $a = -1$) to $y_q \lesssim 0.22 y_b$ (for $a = 0.5$), at the 2σ confidence level. The theoretical uncertainties will change the upper limit of light quark Yukawa couplings from 5% to 14%. We note that the limit for y_q obtained in this way is considerably larger than the results in ref. [42]. It could be understood from our analysis strategy, i.e. in this window, we have $\tau_a > \tau_{\rm min}(a)$, which is far away from the peak region of the signal, while it is not in ref. [42]. From the PYTHIA prediction (see figure 7), we know the typical nonperturbative hadronization effects will shift the peak of angularities by about $\Delta\tau_a \sim 0.01$. Furthermore, the nonperturbative corrections to our predictions for light quark angularities remain small (or within the universal shift region) to considerably smaller values of τ_a. If we push our analysis region a bit more aggressively into the peak region, e.g. to a lower limit of $\tau_a > t_0^g(a) \sim 3.5/125 \times 3^a$, then we obtain the upper limit $y_q \lesssim 0.09 y_b$ at 2σ confidence level for all our choices of a. We can try to be even more aggressive than this, and push the lower limit for τ_a left of the peak of the quark angularity distributions, even though nonperturbative and heavy-quark mass corrections are larger there — this is for illustrative, motivational purposes only. Choosing the analysis region $\tau_a > t_0^q(a) = 1/125 \times 3^a$, we obtain the stronger limit $y_q \lesssim 0.07 y_b$. We summarize the various limits we obtain on y_q for the different analysis windows in table 3. We stress that in this work we have used a simple educated guesses for the quark and gluon shape function parameters, to which this analysis region will be sensitive. If our guesses are close to accurate, though, the above limit is indicative of the power of a single angularity distribution to put a limit on y_q. A definitive limit would require further control of the shape function parameters through universality/scaling arguments and/or extraction from an independent dataset. Alternatively, to further improve the measurements and reduce the impact of the non-perturbative effects, we could use the soft-drop grooming technique [120–122], and this could be considered in a future work. Nevertheless, the potential limits indicated in table 3 show the promise of angularities in separating quark signal from gluon background to obtain strong limits on y_q.

Since the angularities depend on the continuous parameter a, it is also useful to combine the multiple angularity distributions in the analysis. Here we build upon ideas previously developed in [123]. As an example, we show the normalized double differential distributions

JHEP03(2024)123

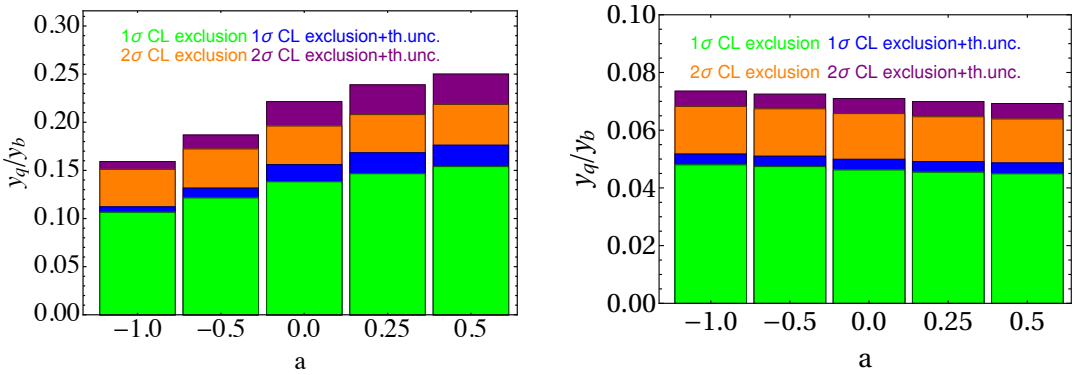

Figure 9. Expected 1σ (green) and 2σ (orange) exclusion limit on Yukawa coupling $y_q(m_H)$ for values of $a = (-1.0, -0.5, 0.0, 0.25, 0.5)$ at NNLL + $\mathcal{O}(\alpha_s)$. y_b is the bottom quark Yukawa coupling in the SM. The impact from theoretical uncertainties are shown with blue (1σ) and purple (2σ) colors. We use the conservative analysis window $\tau_{\min}(a) < \tau_a < \tau_{\max}(a)$ in the left figure, while the more aggressive window $t_0^q(a) < \tau_a < \tau_{\max}(a)$ is used in the right figure.

a	-1.0	-0.5	0.0	0.25	0.5
$[\tau_{\min}(a), \tau_{\max}(a)]$	0.15	0.17	0.20	0.21	0.22
$[t_0^g(a), \tau_{\max}(a)]$	0.085	0.089	0.090	0.088	0.086
$[t_0^q(a), \tau_{\max}(a)]$	0.068	0.067	0.066	0.065	0.064

Table 3. Expected 2σ exclusion limit on Yukawa coupling y_q/y_b for values of $a = \{-1.0, -0.5, 0.0, 0.25, 0.5\}$ at NNLL + $\mathcal{O}(\alpha_s)$ accuracy with different analysis region, with $t_0^g(a) = 3.5/125 \times 3^a$ and $t_0^q(a) = 1/125 \times 3^a$.

of angularities with $a = -1.0$ and $a = 0.5$ from PYTHIA at hadron level for $H \to q\bar{q}$ and $H \to gg$ in figure 10. Performing a likelihood analysis in the regions $\tau_{\min}(a) < \tau_a < \tau_{\max}(a)$ with the same min and max limits for each a as in the single-angularity analysis above, we find that limits on the Yukawa couplings could be further improved about $2\% \sim 3\%$ compared to the single angularity analysis at 2σ confidence level. Although the two different angularities will improve the power of distinguishing the quark and gluon jets, the backgrounds from $H \to b\bar{b}, c\bar{c}$ and $Zq\bar{q}$ will become important since both of them have a similar angularity distributions as the signal. Therefore, the next step to further constraint the light quark Yukawa couplings could be from improving the b-tagging efficiency, detector resolution and so on. If both $H \to b\bar{b}, c\bar{c}$ and $Zq\bar{q}$ could be further reduced about 10 times than current analysis, we estimate that the results from two different angularities could be improved about 12% compared to the single angularity analysis. (Note that these estimates are obtained in our most conservative analysis windows.) Methods for resummation of two angularities have been developed and applied to predictions in [72, 73]. Further development of such predictions for double differential distributions of angularities in Higgs decays and their applications to phenomenology would seem worthwhile.

JHEP03(2024)123

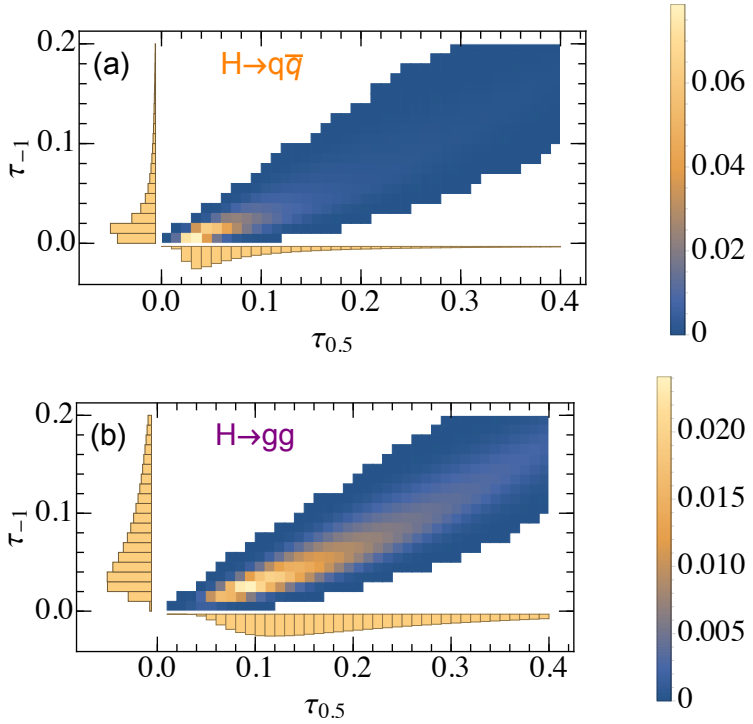

Figure 10. The normalized double differential distributions of two jet angularities $(\tau_{-1.0}, \tau_{0.5})$ from PYTHIA at hadron level for $H \to q\bar{q}$ and $H \to gg$. On the two side axes we show the corresponding single differential spectra. We analyse regions with the same conservative cuts $\tau_{\min}(a) < \tau_a < \tau_{\max}(a)$ for each τ_a as in the one-dimensional analyses used in table 3 to estimate the sensitivity for the y_q.

5 Summary

In this paper, we studied a class of event shape variables angularities from Higgs boson decay at the e^+e^- colliders based on soft-collinear effective theory. Both the quark and gluon final states are calculated to NLL$' + \mathcal{O}(\alpha_s)$ and NNLL $+ \mathcal{O}(\alpha_s)$ accuracy. From NLL$' + \mathcal{O}(\alpha_s)$ to NNLL $+ \mathcal{O}(\alpha_s)$ accuracy, we found a sizable correction for small a angularties. The differential angularity distributions also show a Casimir scaling C_A/C_F from quark to gluon. We compared the predictions resulting from this analysis to PYTHIA at both parton and hadron level, and find good agreement for hadron level results.

Based on the difference of angularity distributions between quark and gluon final state, we proposed to test the light quark Yukawa couplings through angularity distributions at lepton colliders. As an example, we show that the CEPC with $\sqrt{s} = 250$ GeV and an integrated luminosity of 5 ab^{-1} could give a constraint $y_q \lesssim 0.15 - 0.22 y_b$ for $q = u, d, s$, for different values of the angularity parameter a, at 2σ confidence level using a conservative analysis region $[\tau_{\min}(a), \tau_{\max}(a)]$ far away from small τ_a where hadronization and b-mass effects are larger. The theoretical uncertainty for this upper limit is around 10%. In order to further improve the results, it is important to extend the analysis region to small τ_a. It shows that the upper limit could be reduced to $y_q \lesssim 0.09 y_b$, similar to [42], if we push the analysis region down to $[t_0^g(a), \tau_{\max}(a)]$, or even smaller $y_q \lesssim 0.07 y_b$ in the region $[t_0^q(a), \tau_{\max}(a)]$. However,

JHEP03(2024)123

the theoretical prediction in the small τ_a region is strongly dependent on the non-perturbative model assumptions and this issue could be overcome by gaining better knowledge of the gluon soft shape function, in particular, or by utilizing soft-drop grooming techniques. Utilizing multiple angularities at once also shows promise in improving the potential limit on y_q further.

Note. As this paper was being finalized, ref. [61] appeared, computing Higgs angularity distributions to NNLL$'$ resummed and NLO fixed-order accuracy. We have not yet compared to the technical results of this paper; here we have focused more extensively on the phenomenological application of the results to the determination of Yukawa couplings.

Acknowledgments

BY would like to thank Zhongbo Kang and C.-P. Yuan for useful discussions, and Wan-Li Ju for discussions about the calculation of thrust in Higgs decay. This material is based upon work supported by the U.S. Department of Energy, Office of Science, Office of Nuclear Physics, and through an Early Career Research Award. Portions of the work were also supported by the Laboratory Directed Research and Development program of Los Alamos National Laboratory under project numbers 20190033ER and 20200775PRD4. Los Alamos National Laboratory is operated by Triad National Security, LLC, for the National Nuclear Security Administration of U.S. Department of Energy (Contract No. 89233218CNA000001). BY is also supported by the IHEP under Contract No. E25153U1.

A Angularity distributions in Higgs decay to $\mathcal{O}(\alpha_s)$

In this section, we give details of the calculation of the full QCD prediction for angularity τ_a distribution away from $\tau_a = 0$. This follows closely the similar calculation given in [70]. Both the virtual and real diagrams can contribute to the angularity τ_a distribution at $\mathcal{O}(\alpha_s)$. However, the virtual diagram is proportional to $\delta(\tau_a)$, which is fully accounted for in the SCET prediction for the singular terms given by eq. (2.28). Here we only need to consider the terms contributing the difference between full QCD and SCET given by eq. (2.31). So we only need to consider the real diagram's contribution,

$$\frac{1}{\Gamma^i_{H0}}\frac{d\Gamma^i_H}{d\tau_a}\bigg|_{\text{QCD}} = \left(\frac{\alpha_s}{2\pi}\right) A^i_a(\tau_a). \tag{A.1}$$

For Higgs decaying to quark state, the coefficient $A^q_a(\tau_a)$ is,

$$A^q_a(\tau_a) = C_F \int dx_1 dx_2 \frac{(1-x_1)^2 + (1-x_2)^2 + 2x_1x_2}{(1-x_1)(1-x_2)} \delta(\tau_a - \tau_a(x_1, x_2)), \tag{A.2}$$

where $x_{1,2} \equiv 2E_{1,2}/m_H$ are the energy fractions of any two of the three final state partons.

There are two subprocesses $H \to gg(\to q\bar{q})$ and $H \to ggg$ that can contribute to $A^g_a(\tau_a)$. For $H \to gg(\to q\bar{q})$ channel we have,

$$A^{gq\bar{q}}_a(\tau_a) = N_f \int dx_1 dx_2 \frac{x_1^2 + x_2^2 - 2x_1 - 2x_2 + 2}{x_1 + x_2 - 1} \delta(\tau_a - \tau_a(x_1, x_2)). \tag{A.3}$$

JHEP03(2024)123

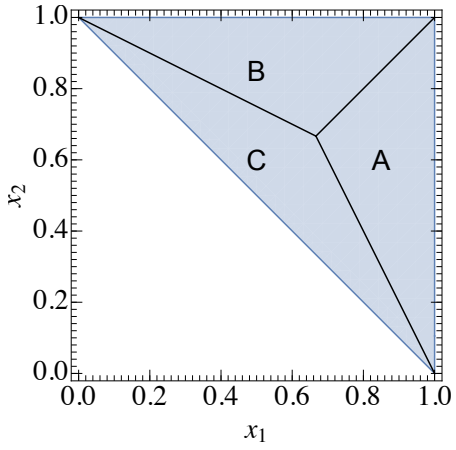

Figure 11. The three body phase space. The parameter x_i is defined as $x_i = 2E_i/m_H$ and $x_1 + x_2 + x_3 = 2$.

For $H \to ggg$,

$$A_a^{ggg}(\tau_a) = C_A \int dx_1 dx_2 \frac{1+(1-x_1)^4+(1-x_2)^4+(1-x_1-x_2)^4}{3(1-x_1)(1-x_2)(x_1+x_2-1)} \delta(\tau_a - \tau_a(x_1, x_2)). \tag{A.4}$$

The coefficient $A_a^g(\tau_a) = A_a^{gq\bar{q}}(\tau_a) + A_a^{ggg}(\tau_a)$.

The thrust axis in these 3-body final states is always along the direction of the particle with the largest energy. Therefore, the phase space in the x_1, x_2 plane can divided into three regions, as shown in figure 11. The value of the angularity $\tau_a(x_1, x_2)$ is dependent on which parton has the largest energy. In a region where $x_i > x_{j,k}$, the angularity $\tau_a(x_1, x_2)$ is given by,

$$\tau_a(x_1, x_2)\Big|_{x_i > x_{j,k}} = \frac{1}{x_i}(1-x_i)^{1-a/2}\left[(1-x_j)^{1-a/2}(1-x_k)^{a/2} + (1-x_k)^{1-a/2}(1-x_j)^{a/2}\right]. \tag{A.5}$$

In the following, we will use phase space region C where $x_3 > x_{1,2}$ as an example to discuss the calculation of $A_a^i(\tau_a)$. The integration in phase space A and B can be related to the integration over region C by the appropriate change of variables. The angularity in phase space C can be written as,

$$\tau_a = \frac{1}{2-x_1-x_2}(x_1+x_2-1)^{1-a/2}\left[(1-x_1)^{1-a/2}(1-x_2)^{a/2} + (1-x_2)^{1-a/2}(1-x_1)^{a/2}\right]. \tag{A.6}$$

It turns out to be convenient to change the integration variables from x_1, x_2 to τ_a and w, where

$$w = \frac{1-x_1}{2-x_1-x_2}. \tag{A.7}$$

Therefore, x_1 and x_2 are given by,

$$\begin{aligned} x_1(w, \tau_a) &= 1 - w + w\left[\frac{\tau_a}{w^{1-a/2}(1-w)^{a/2} + w^{a/2}(1-w)^{1-a/2}}\right]^{\frac{1}{1-a/2}}, \\ x_2(w, \tau_a) &= x_1(1-w, \tau_a). \end{aligned} \tag{A.8}$$

JHEP03(2024)123

In the phase space region C, we have

$$x_1(w,\tau_a) \le 2 - x_1(w,\tau_a) - x_2(w,\tau_a), \quad x_2(w,\tau_a) \le 2 - x_1(w,\tau_a) - x_2(w,\tau_a) \tag{A.9}$$

The integration region of w is determined by solving these inequalities, which are equivalent to the conditions,

$$\tau_a = F_a(w_{\min}), \quad \tau_a = F_a(1 - w_{\max}), \tag{A.10}$$

whose solutions give the lower and upper limits of the integral over w, $w_{\min}$ and $w_{\max}$, respectively, where the function F_a is given by

$$F_a(w) = \frac{w(1-w)^{a/2}}{(1+w)^{1-a/2}}(w^{1-a} + (1-w)^{1-a}). \tag{A.11}$$

These limits are themselves functions of τ_a, and cease to have a solution above the maximally allowed value of $\tau_a = \tau_a^{\max}$, which is $\tau_a^{\max} = (1/3)^{1-a/2}$ at $\mathcal{O}(\alpha_s)$.[2] Then, for example, the integral for A_a^q in eq. (A.2) is expressed:

$$A_a^q(\tau_a) = C_F \int_{w_{\min}(\tau_a)}^{w_{\max}(\tau_a)} dw\, J(w,\tau_a) \left[\frac{x_1^2 + x_2^2}{(1-x_1)(1-x_2)} + 2\frac{x_1^2 + x_3^2}{(1-x_1)(1-x_3)} \right]_{x_{1,2}=x_{1,2}(w,\tau_a)}, \tag{A.12}$$

where $x_{1,2}$ are expressed in the form eq. (A.8), and $x_3 = 2 - x_1 - x_2$. The factor J is the Jacobian associated with the variable transformation eq. (A.8),

$$J(w,\tau_a) = \left| \begin{matrix} \frac{\partial x_1}{\partial w} & \frac{\partial x_1}{\partial \tau} \\ \frac{\partial x_2}{\partial w} & \frac{\partial x_2}{\partial \tau} \end{matrix} \right|. \tag{A.13}$$

The endpoints $w_{\min,\max}$ in eq. (A.10), the Jacobian eq. (A.13), and the integral eq. (A.12) are all easily evaluated numerically, which is how we have computed the A_a^i's and the resulting remainder functions illustrated in, e.g. figure 1. The gluon channel contributions A_a^g given by eqs. (A.3) and (A.4) are expressed and evaluated similarly to eq. (A.12).

B Ingredients for NNLL resummation

In this appendix we collect results needed to compute angularity distributions to NNLL accuracy. The coefficients of β function in the $\overline{\text{MS}}$ scheme are given by [124–126],

$$\begin{aligned} \beta_0 &= \frac{11}{3}C_A - \frac{4}{3}T_F n_f, \\ \beta_1 &= \frac{34}{3}C_A^2 - \left(\frac{20}{3}C_A + 4C_F\right) T_F n_f, \\ \beta_2 &= \frac{2857}{54}C_A^3 + \left(C_F^2 - \frac{205}{18}C_F C_A - \frac{1415}{54}C_A^2\right) 2T_F n_f + \left(\frac{11}{9}C_F + \frac{79}{54}C_A\right) 4T_F^2 n_f^2 \,., \end{aligned} \tag{B.1}$$

[2] This is true at least for values of $a \gtrsim -2$. See [70] for subtleties for smaller values of a.

JHEP03(2024)123

and the coefficients of the anomalous dimension γ_y of the Yukawa coupling y_q in eq. (2.12) are given by [127]:

$$\begin{aligned}\gamma_y^0 &= 6C_F,\\ \gamma_y^1 &= 3C_F^2 + \frac{97}{3}C_A C_F - \frac{10}{3}C_F n_f.\end{aligned} \tag{B.2}$$

The cusp anomalous dimensions up to 3-loop order [128, 129]

$$\begin{aligned}\Gamma_0^i &= 4C_i,\\ \Gamma_1^i &= \left[\left(\frac{67}{9}-\frac{\pi^2}{3}\right)C_A - \frac{20}{9}T_F N_f\right]\Gamma_0^i,\\ \Gamma_2^i &= \left[\left(\frac{245}{6}-\frac{134\pi^2}{27}+\frac{11\pi^4}{45}+\frac{22\zeta_3}{3}\right)C_A^2 + \left(-\frac{418}{27}+\frac{40\pi^2}{27}-\frac{56\zeta_3}{3}\right)C_A T_F n_f\right.\\ &\quad \left. + \left(-\frac{55}{3}+16\zeta_3\right)C_F T_F n_f - \frac{16}{27}T_F^2 n_f^2\right]\Gamma_0^i.\end{aligned} \tag{B.3}$$

The non-cusp anomalous dimension for the hard function up to 2-loop level [84, 101, 130–133],

$$\begin{aligned}\gamma_{H0}^q &= -12C_F,\\ \gamma_{H1}^q &= -2C_F\left[\left(\frac{82}{9}-52\zeta_3\right)C_A + (3-4\pi^2+48\zeta_3)C_F + \left(\frac{65}{9}+\pi^2\right)\beta_0\right],\\ \gamma_{H0}^g &= -4\beta_0,\\ \gamma_{H1}^g &= \left(-\frac{236}{9}+2\zeta_3\right)C_A^2 + \left(-\frac{76}{9}+\frac{2\pi^2}{3}\right)C_A\beta_0 - 4\beta_1.\end{aligned} \tag{B.4}$$

The 1-loop soft non-cusp anomalous dimension is zero, e.g. $\gamma_{S0}^i(a) = 0$. The 2-loop jet and soft anomalous dimensions are not known analytically, but are related by $\gamma_H^i + \gamma_J^i(a) + \gamma_S^i(a) = 0$, and $\gamma_S^i(a)$ is known in numerically integrable form to 2-loop order, thanks to [88]. The 2-loop soft anomalous dimension can be written in the form

$$\gamma_{S1}^i(a) = \frac{2C_i}{1-a}\left[\gamma_1^{CA}C_A + \gamma_1^{nf}(a)T_F n_f\right], \tag{B.5}$$

where

$$\begin{aligned}\gamma_1^{CA}(a) &= -\frac{808}{27}+\frac{11\pi^2}{9}+28\zeta_3 - \Delta\gamma_1^{CA}(a)\\ \gamma_1^{nf}(a) &= \frac{224}{27}-\frac{4\pi^2}{9} - \Delta\gamma_1^{nf}(a),\end{aligned} \tag{B.6}$$

where the deviations from the $a = 0$ values shown are given by the integrals:

$$\begin{aligned}\Delta\gamma_1^{CA}(a) &= \int_0^1 dx\int_0^1 dy\,\frac{32x^2(1+xy+y^2)\left[x(1+y^2)+(x+y)(1+xy)\right]}{y(1-x^2)(x+y)^2(1+xy)^2}\ln\left[\frac{(x^a+xy)(x+x^a y)}{x^a(1+xy)(x+y)}\right],\\ \Delta\gamma_1^{nf}(a) &= \int_0^1 dx\int_0^1 dy\,\frac{64x^2(1+y^2)}{(1-x^2)(x+y)^2(1+xy)^2}\ln\left[\frac{(x^a+xy)(x+x^a y)}{x^a(1+xy)(x+y)}\right],\end{aligned} \tag{B.7}$$

which vanish for $a = 0$. The integral representations can easily be evaluated numerically to high accuracy for any value of a, and the relevant values for our work are given in table 4.

JHEP03(2024)123

a	-1.0	-0.5	0.0	0.25	0.5
γ_1^{CA}	1.0417	9.8976	15.795	17.761	19.132
γ_1^{nf}	-0.9571	1.8440	3.9098	4.6398	5.1613

Table 4. Coefficients of the two-loop soft anomalous dimension as defined in eq. (B.5).

Open Access. This article is distributed under the terms of the Creative Commons Attribution License (CC-BY4.0), which permits any use, distribution and reproduction in any medium, provided the original author(s) and source are credited.

References

[1] ATLAS collaboration, *Observation of a new particle in the search for the Standard Model Higgs boson with the ATLAS detector at the LHC*, *Phys. Lett. B* **716** (2012) 1 [arXiv:1207.7214] [INSPIRE].

[2] CMS collaboration, *Observation of a New Boson at a Mass of* 125 *GeV with the CMS Experiment at the LHC*, *Phys. Lett. B* **716** (2012) 30 [arXiv:1207.7235] [INSPIRE].

[3] S. Bar-Shalom and A. Soni, *Universally enhanced light-quarks Yukawa couplings paradigm*, *Phys. Rev. D* **98** (2018) 055001 [arXiv:1804.02400] [INSPIRE].

[4] G.T. Bodwin, F. Petriello, S. Stoynev and M. Velasco, *Higgs boson decays to quarkonia and the $H\bar{c}c$ coupling*, *Phys. Rev. D* **88** (2013) 053003 [arXiv:1306.5770] [INSPIRE].

[5] A.L. Kagan et al., *Exclusive Window onto Higgs Yukawa Couplings*, *Phys. Rev. Lett.* **114** (2015) 101802 [arXiv:1406.1722] [INSPIRE].

[6] T. Han, A.K. Leibovich, Y. Ma and X.-Z. Tan, *Higgs boson decay to charmonia via c-quark fragmentation*, *JHEP* **08** (2022) 073 [arXiv:2202.08273] [INSPIRE].

[7] I. Brivio, F. Goertz and G. Isidori, *Probing the Charm Quark Yukawa Coupling in Higgs+Charm Production*, *Phys. Rev. Lett.* **115** (2015) 211801 [arXiv:1507.02916] [INSPIRE].

[8] G. Perez, Y. Soreq, E. Stamou and K. Tobioka, *Constraining the charm Yukawa and Higgs-quark coupling universality*, *Phys. Rev. D* **92** (2015) 033016 [arXiv:1503.00290] [INSPIRE].

[9] Y. Zhou, *Constraining the Higgs boson coupling to light quarks in the H→ZZ final states*, *Phys. Rev. D* **93** (2016) 013019 [arXiv:1505.06369] [INSPIRE].

[10] G. Perez, Y. Soreq, E. Stamou and K. Tobioka, *Prospects for measuring the Higgs boson coupling to light quarks*, *Phys. Rev. D* **93** (2016) 013001 [arXiv:1505.06689] [INSPIRE].

[11] J. de Blas et al., *Higgs Boson Studies at Future Particle Colliders*, *JHEP* **01** (2020) 139 [arXiv:1905.03764] [INSPIRE].

[12] F. Bishara, U. Haisch, P.F. Monni and E. Re, *Constraining Light-Quark Yukawa Couplings from Higgs Distributions*, *Phys. Rev. Lett.* **118** (2017) 121801 [arXiv:1606.09253] [INSPIRE].

[13] Y. Soreq, H.X. Zhu and J. Zupan, *Light quark Yukawa couplings from Higgs kinematics*, *JHEP* **12** (2016) 045 [arXiv:1606.09621] [INSPIRE].

[14] G. Bonner and H.E. Logan, *Constraining the Higgs couplings to up and down quarks using production kinematics at the CERN Large Hadron Collider*, arXiv:1608.04376 [INSPIRE].

JHEP03(2024)123

[15] W. Bizoń et al., *Fiducial distributions in Higgs and Drell-Yan production at N^3LL+NNLO*, *JHEP* **12** (2018) 132 [arXiv:1805.05916] [INSPIRE].

[16] X. Chen et al., *Precise QCD Description of the Higgs Boson Transverse Momentum Spectrum*, *Phys. Lett. B* **788** (2019) 425 [arXiv:1805.00736] [INSPIRE].

[17] G. Billis et al., *Higgs pT Spectrum and Total Cross Section with Fiducial Cuts at Third Resummed and Fixed Order in QCD*, *Phys. Rev. Lett.* **127** (2021) 072001 [arXiv:2102.08039] [INSPIRE].

[18] L. Alasfar et al., *Machine learning the trilinear and light-quark Yukawa couplings from Higgs pair kinematic shapes*, *JHEP* **11** (2022) 045 [arXiv:2207.04157] [INSPIRE].

[19] N. Vignaroli, *Off-Shell Probes of the Higgs Yukawa Couplings: Light Quarks and Charm*, *Symmetry* **14** (2022) 1183 [arXiv:2205.09449] [INSPIRE].

[20] E. Balzani, R. Gröber and M. Vitti, *Light-quark Yukawa couplings from off-shell Higgs production*, *JHEP* **10** (2023) 027 [arXiv:2304.09772] [INSPIRE].

[21] A. Falkowski et al., *Light quark Yukawas in triboson final states*, *JHEP* **04** (2021) 023 [arXiv:2011.09551] [INSPIRE].

[22] CEPC Study Group collaboration, *CEPC Conceptual Design Report: Volume 2 — Physics & Detector*, arXiv:1811.10545 [INSPIRE].

[23] ILC collaboration, *The International Linear Collider Technical Design Report — Volume 2: Physics*, arXiv:1306.6352 [INSPIRE].

[24] CLIC collaboration, *The CLIC Potential for New Physics*, arXiv:1812.02093 [DOI:10.23731/CYRM-2018-003] [INSPIRE].

[25] FCC collaboration, *FCC-ee: The Lepton Collider: Future Circular Collider Conceptual Design Report Volume 2*, *Eur. Phys. J. ST* **228** (2019) 261 [INSPIRE].

[26] Z. Fodor, *How to See the Differences Between Quark and Gluon Jets*, *Phys. Rev. D* **41** (1990) 1726 [INSPIRE].

[27] J. Pumplin, *How to tell quark jets from gluon jets*, *Phys. Rev. D* **44** (1991) 2025 [INSPIRE].

[28] J. Gallicchio and M.D. Schwartz, *Quark and Gluon Tagging at the LHC*, *Phys. Rev. Lett.* **107** (2011) 172001 [arXiv:1106.3076] [INSPIRE].

[29] J. Gallicchio and M.D. Schwartz, *Quark and Gluon Jet Substructure*, *JHEP* **04** (2013) 090 [arXiv:1211.7038] [INSPIRE].

[30] A.J. Larkoski, J. Thaler and W.J. Waalewijn, *Gaining (Mutual) Information about Quark/Gluon Discrimination*, *JHEP* **11** (2014) 129 [arXiv:1408.3122] [INSPIRE].

[31] B. Bhattacherjee et al., *Associated jet and subjet rates in light-quark and gluon jet discrimination*, *JHEP* **04** (2015) 131 [arXiv:1501.04794] [INSPIRE].

[32] P. Gras et al., *Systematics of quark/gluon tagging*, *JHEP* **07** (2017) 091 [arXiv:1704.03878] [INSPIRE].

[33] Y.-T. Chien and I.W. Stewart, *Collinear Drop*, *JHEP* **06** (2020) 064 [arXiv:1907.11107] [INSPIRE].

[34] H.T. Li, B. Yan and C.-P. Yuan, *Discriminating between Higgs Production Mechanisms via Jet Charge at the LHC*, *Phys. Rev. Lett.* **131** (2023) 041802 [arXiv:2301.07914] [INSPIRE].

[35] X.-R. Wang and B. Yan, *Probing the Hgg coupling through the jet charge correlation in Higgs boson decay*, *Phys. Rev. D* **108** (2023) 056010 [arXiv:2302.02084] [INSPIRE].

JHEP03(2024)123

[36] E.M. Metodiev and J. Thaler, *Jet Topics: Disentangling Quarks and Gluons at Colliders*, *Phys. Rev. Lett.* **120** (2018) 241602 [arXiv:1802.00008] [INSPIRE].

[37] M. Dasgupta and G.P. Salam, *Event shapes in e^+e^- annihilation and deep inelastic scattering*, *J. Phys. G* **30** (2004) R143 [hep-ph/0312283] [INSPIRE].

[38] T. Becher and M.D. Schwartz, *A precise determination of α_s from LEP thrust data using effective field theory*, *JHEP* **07** (2008) 034 [arXiv:0803.0342] [INSPIRE].

[39] R. Abbate et al., *Thrust at N^3LL with Power Corrections and a Precision Global Fit for $\alpha_s(mZ)$*, *Phys. Rev. D* **83** (2011) 074021 [arXiv:1006.3080] [INSPIRE].

[40] P.F. Monni, T. Gehrmann and G. Luisoni, *Two-Loop Soft Corrections and Resummation of the Thrust Distribution in the Dijet Region*, *JHEP* **08** (2011) 010 [arXiv:1105.4560] [INSPIRE].

[41] A.H. Hoang, D.W. Kolodrubetz, V. Mateu and I.W. Stewart, *C-parameter distribution at N^3LL' including power corrections*, *Phys. Rev. D* **91** (2015) 094017 [arXiv:1411.6633] [INSPIRE].

[42] J. Gao, *Probing light-quark Yukawa couplings via hadronic event shapes at lepton colliders*, *JHEP* **01** (2018) 038 [arXiv:1608.01746] [INSPIRE].

[43] E. Farhi, *A QCD Test for Jets*, *Phys. Rev. Lett.* **39** (1977) 1587 [INSPIRE].

[44] T. Chandramohan and L. Clavelli, *Consequences of Second Order QCD for Jet Structure in e^+e^- Annihilation*, *Nucl. Phys. B* **184** (1981) 365 [INSPIRE].

[45] L. Clavelli and D. Wyler, *Kinematical Bounds on Jet Variables and the Heavy Jet Mass Distribution*, *Phys. Lett. B* **103** (1981) 383 [INSPIRE].

[46] G. Parisi, *Super Inclusive Cross-Sections*, *Phys. Lett. B* **74** (1978) 65 [INSPIRE].

[47] J.F. Donoghue, F.E. Low and S.-Y. Pi, *Tensor Analysis of Hadronic Jets in Quantum Chromodynamics*, *Phys. Rev. D* **20** (1979) 2759 [INSPIRE].

[48] S. Catani, G. Turnock and B.R. Webber, *Jet broadening measures in e^+e^- annihilation*, *Phys. Lett. B* **295** (1992) 269 [INSPIRE].

[49] S. Catani et al., *New clustering algorithm for multi-jet cross-sections in e^+e^- annihilation*, *Phys. Lett. B* **269** (1991) 432 [INSPIRE].

[50] M.H. Seymour, *Jet shapes in hadron collisions: Higher orders, resummation and hadronization*, *Nucl. Phys. B* **513** (1998) 269 [hep-ph/9707338] [INSPIRE].

[51] J. Isaacson, H.-N. Li, Z. Li and C.-P. Yuan, *Factorization for substructures of boosted Higgs jets*, *Phys. Lett. B* **771** (2017) 619 [arXiv:1505.06368] [INSPIRE].

[52] G. Li et al., *Probing the Higgs boson-gluon coupling via the jet energy profile at e^+e^- colliders*, *Phys. Rev. D* **98** (2018) 076010 [arXiv:1805.10138] [INSPIRE].

[53] H.-N. Li, Z. Li and C.-P. Yuan, *QCD resummation for jet substructures*, *Phys. Rev. Lett.* **107** (2011) 152001 [arXiv:1107.4535] [INSPIRE].

[54] Y.-T. Chien and M.D. Schwartz, *Resummation of heavy jet mass and comparison to LEP data*, *JHEP* **08** (2010) 058 [arXiv:1005.1644] [INSPIRE].

[55] J. Gao, Y. Gong, W.-L. Ju and L.L. Yang, *Thrust distribution in Higgs decays at the next-to-leading order and beyond*, *JHEP* **03** (2019) 030 [arXiv:1901.02253] [INSPIRE].

[56] M.-X. Luo, V. Shtabovenko, T.-Z. Yang and H.X. Zhu, *Analytic Next-To-Leading Order Calculation of Energy-Energy Correlation in Gluon-Initiated Higgs Decays*, *JHEP* **06** (2019) 037 [arXiv:1903.07277] [INSPIRE].

JHEP03(2024)123

[57] S. Alioli et al., *Resummed predictions for hadronic Higgs boson decays*, *JHEP* **04** (2021) 254 [arXiv:2009.13533] [INSPIRE].

[58] W.-L. Ju, Y. Xu, L.L. Yang and B. Zhou, *Thrust distribution in Higgs decays up to the fifth logarithmic order*, *Phys. Rev. D* **107** (2023) 114034 [arXiv:2301.04294] [INSPIRE].

[59] C.F. Berger, T. Kucs and G.F. Sterman, *Event shape/energy flow correlations*, *Phys. Rev. D* **68** (2003) 014012 [hep-ph/0303051] [INSPIRE].

[60] G. Bell, A. Hornig, C. Lee and J. Talbert, e^+e^- *angularity distributions at NNLL′ accuracy*, *JHEP* **01** (2019) 147 [arXiv:1808.07867] [INSPIRE].

[61] J. Zhu et al., *Angularity in Higgs boson decays via* $H \to gg$ *at NNLL′ accuracy*, arXiv:2311.07282 [INSPIRE].

[62] C.F. Berger and G.F. Sterman, *Scaling rule for nonperturbative radiation in a class of event shapes*, *JHEP* **09** (2003) 058 [hep-ph/0307394] [INSPIRE].

[63] S. Brandt, C. Peyrou, R. Sosnowski and A. Wroblewski, *The principal axis of jets. An attempt to analyze high-energy collisions as two-body processes*, *Phys. Lett.* **12** (1964) 57 [INSPIRE].

[64] Y.L. Dokshitzer, A. Lucenti, G. Marchesini and G.P. Salam, *On the QCD analysis of jet broadening*, *JHEP* **01** (1998) 011 [hep-ph/9801324] [INSPIRE].

[65] T. Becher, G. Bell and M. Neubert, *Factorization and Resummation for Jet Broadening*, *Phys. Lett. B* **704** (2011) 276 [arXiv:1104.4108] [INSPIRE].

[66] J.-Y. Chiu, A. Jain, D. Neill and I.Z. Rothstein, *The Rapidity Renormalization Group*, *Phys. Rev. Lett.* **108** (2012) 151601 [arXiv:1104.0881] [INSPIRE].

[67] J.-Y. Chiu, A. Jain, D. Neill and I.Z. Rothstein, *A Formalism for the Systematic Treatment of Rapidity Logarithms in Quantum Field Theory*, *JHEP* **05** (2012) 084 [arXiv:1202.0814] [INSPIRE].

[68] A. Budhraja, A. Jain and M. Procura, *One-loop angularity distributions with recoil using Soft-Collinear Effective Theory*, *JHEP* **08** (2019) 144 [arXiv:1903.11087] [INSPIRE].

[69] C.W. Bauer, S.P. Fleming, C. Lee and G.F. Sterman, *Factorization of* e^+e^- *Event Shape Distributions with Hadronic Final States in Soft Collinear Effective Theory*, *Phys. Rev. D* **78** (2008) 034027 [arXiv:0801.4569] [INSPIRE].

[70] A. Hornig, C. Lee and G. Ovanesyan, *Effective Predictions of Event Shapes: Factorized, Resummed, and Gapped Angularity Distributions*, *JHEP* **05** (2009) 122 [arXiv:0901.3780] [INSPIRE].

[71] S.D. Ellis et al., *Jet Shapes and Jet Algorithms in SCET*, *JHEP* **11** (2010) 101 [arXiv:1001.0014] [INSPIRE].

[72] A.J. Larkoski, I. Moult and D. Neill, *Toward Multi-Differential Cross Sections: Measuring Two Angularities on a Single Jet*, *JHEP* **09** (2014) 046 [arXiv:1401.4458] [INSPIRE].

[73] M. Procura, W.J. Waalewijn and L. Zeune, *Joint resummation of two angularities at next-to-next-to-leading logarithmic order*, *JHEP* **10** (2018) 098 [arXiv:1806.10622] [INSPIRE].

[74] C.W. Bauer, S. Fleming and M.E. Luke, *Summing Sudakov logarithms in* $B \to X_s\gamma$ *in effective field theory*, *Phys. Rev. D* **63** (2000) 014006 [hep-ph/0005275] [INSPIRE].

[75] C.W. Bauer, S. Fleming, D. Pirjol and I.W. Stewart, *An effective field theory for collinear and soft gluons: Heavy to light decays*, *Phys. Rev. D* **63** (2001) 114020 [hep-ph/0011336] [INSPIRE].

JHEP03(2024)123

[76] C.W. Bauer and I.W. Stewart, *Invariant operators in collinear effective theory*, *Phys. Lett. B* **516** (2001) 134 [hep-ph/0107001] [INSPIRE].

[77] C.W. Bauer, D. Pirjol and I.W. Stewart, *Soft collinear factorization in effective field theory*, *Phys. Rev. D* **65** (2002) 054022 [hep-ph/0109045] [INSPIRE].

[78] L.G. Almeida et al., *Comparing and counting logs in direct and effective methods of QCD resummation*, *JHEP* **04** (2014) 174 [arXiv:1401.4460] [INSPIRE].

[79] G.P. Korchemsky and G. Marchesini, *Resummation of large infrared corrections using Wilson loops*, *Phys. Lett. B* **313** (1993) 433 [INSPIRE].

[80] N.A. Sveshnikov and F.V. Tkachov, *Jets and quantum field theory*, *Phys. Lett. B* **382** (1996) 403 [hep-ph/9512370] [INSPIRE].

[81] P.S. Cherzor and N.A. Sveshnikov, *Jet observables and energy momentum tensor*, in the proceedings of the *12th International Workshop on High-Energy Physics and Quantum Field Theory (QFTHEP 97)*, Samara, Russian Federation, September 04–10 (1997) [hep-ph/9710349] [INSPIRE].

[82] A.V. Belitsky, G.P. Korchemsky and G.F. Sterman, *Energy flow in QCD and event shape functions*, *Phys. Lett. B* **515** (2001) 297 [hep-ph/0106308] [INSPIRE].

[83] H. Contopanagos, E. Laenen and G.F. Sterman, *Sudakov factorization and resummation*, *Nucl. Phys. B* **484** (1997) 303 [hep-ph/9604313] [INSPIRE].

[84] C.F. Berger et al., *Higgs Production with a Central Jet Veto at NNLL+NNLO*, *JHEP* **04** (2011) 092 [arXiv:1012.4480] [INSPIRE].

[85] S. Fleming, A.H. Hoang, S. Mantry and I.W. Stewart, *Top Jets in the Peak Region: Factorization Analysis with NLL Resummation*, *Phys. Rev. D* **77** (2008) 114003 [arXiv:0711.2079] [INSPIRE].

[86] R. Kelley, M.D. Schwartz, R.M. Schabinger and H.X. Zhu, *The two-loop hemisphere soft function*, *Phys. Rev. D* **84** (2011) 045022 [arXiv:1105.3676] [INSPIRE].

[87] G. Bell, R. Rahn and J. Talbert, *Automated Calculation of Dijet Soft Functions in Soft-Collinear Effective Theory*, *PoS* **RADCOR2015** (2016) 052 [arXiv:1512.06100] [INSPIRE].

[88] G. Bell, R. Rahn and J. Talbert, *Two-loop anomalous dimensions of generic dijet soft functions*, *Nucl. Phys. B* **936** (2018) 520 [arXiv:1805.12414] [INSPIRE].

[89] G. Bell, R. Rahn and J. Talbert, *Generic dijet soft functions at two-loop order: correlated emissions*, *JHEP* **07** (2019) 101 [arXiv:1812.08690] [INSPIRE].

[90] D. Kang, O.Z. Labun and C. Lee, *Equality of hemisphere soft functions for e^+e^-, DIS and pp collisions at $\mathcal{O}(\alpha_s^2)$*, *Phys. Lett. B* **748** (2015) 45 [arXiv:1504.04006] [INSPIRE].

[91] C.W. Bauer and A.V. Manohar, *Shape function effects in $\vec{B} \to X_s\gamma$ and $\vec{B} \to X_u l\bar{\nu}u$ decays*, *Phys. Rev. D* **70** (2004) 034024 [hep-ph/0312109] [INSPIRE].

[92] T. Becher and M.D. Schwartz, *Direct photon production with effective field theory*, *JHEP* **02** (2010) 040 [arXiv:0911.0681] [INSPIRE].

[93] T. Becher and M. Neubert, *Toward a NNLO calculation of the anti-B → X(s) gamma decay rate with a cut on photon energy. II. Two-loop result for the jet function*, *Phys. Lett. B* **637** (2006) 251 [hep-ph/0603140] [INSPIRE].

[94] T. Becher and G. Bell, *The gluon jet function at two-loop order*, *Phys. Lett. B* **695** (2011) 252 [arXiv:1008.1936] [INSPIRE].

JHEP03(2024)123

[95] R. Brüser, Z.L. Liu and M. Stahlhofen, *Three-Loop Quark Jet Function*, *Phys. Rev. Lett.* **121** (2018) 072003 [arXiv:1804.09722] [INSPIRE].

[96] P. Banerjee, P.K. Dhani and V. Ravindran, *Gluon jet function at three loops in QCD*, *Phys. Rev. D* **98** (2018) 094016 [arXiv:1805.02637] [INSPIRE].

[97] A. Hornig, Y. Makris and T. Mehen, *Jet Shapes in Dijet Events at the LHC in SCET*, *JHEP* **04** (2016) 097 [arXiv:1601.01319] [INSPIRE].

[98] S. Catani and M.H. Seymour, *The dipole formalism for the calculation of QCD jet cross-sections at next-to-leading order*, *Phys. Lett. B* **378** (1996) 287 [hep-ph/9602277] [INSPIRE].

[99] S. Catani and M.H. Seymour, *A general algorithm for calculating jet cross-sections in NLO QCD*, *Nucl. Phys. B* **485** (1997) 291 [hep-ph/9605323] [INSPIRE].

[100] G. Bell, K. Brune, G. Das and M. Wald, *Automation of Beam and Jet functions at NNLO*, *SciPost Phys. Proc.* **7** (2022) 021 [arXiv:2110.04804] [INSPIRE].

[101] T. Becher, M. Neubert and B.D. Pecjak, *Factorization and Momentum-Space Resummation in Deep-Inelastic Scattering*, *JHEP* **01** (2007) 076 [hep-ph/0607228] [INSPIRE].

[102] T. Becher and M. Neubert, *Threshold resummation in momentum space from effective field theory*, *Phys. Rev. Lett.* **97** (2006) 082001 [hep-ph/0605050] [INSPIRE].

[103] R.K. Ellis, W.J. Stirling and B.R. Webber, *QCD and collider physics*, Cambridge University Press, (2011) [DOI:10.1017/cbo9780511628788].

[104] A. Djouadi, *The anatomy of electro-weak symmetry breaking. I: The Higgs boson in the standard model*, *Phys. Rept.* **457** (2008) 1 [hep-ph/0503172] [INSPIRE].

[105] G.P. Korchemsky, *Shape functions and power corrections to the event shapes*, in the proceedings of the *3rd Workshop on Continuous Advances in QCD (QCD 98)*, Les Arcs, France, March 21–28 (1998) [hep-ph/9806537] [INSPIRE].

[106] G.P. Korchemsky and G.F. Sterman, *Power corrections to event shapes and factorization*, *Nucl. Phys. B* **555** (1999) 335 [hep-ph/9902341] [INSPIRE].

[107] A.H. Hoang and I.W. Stewart, *Designing gapped soft functions for jet production*, *Phys. Lett. B* **660** (2008) 483 [arXiv:0709.3519] [INSPIRE].

[108] C. Lee and G.F. Sterman, *Momentum Flow Correlations from Event Shapes: Factorized Soft Gluons and Soft-Collinear Effective Theory*, *Phys. Rev. D* **75** (2007) 014022 [hep-ph/0611061] [INSPIRE].

[109] Z. Ligeti, I.W. Stewart and F.J. Tackmann, *Treating the b quark distribution function with reliable uncertainties*, *Phys. Rev. D* **78** (2008) 114014 [arXiv:0807.1926] [INSPIRE].

[110] A.H. Hoang and S. Kluth, *Hemisphere Soft Function at $O(\alpha_s^2)$ for Dijet Production in e^+e^- Annihilation*, arXiv:0806.3852 [INSPIRE].

[111] B. Bachu et al., *Boosted top quarks in the peak region with N^3LL resummation*, *Phys. Rev. D* **104** (2021) 014026 [arXiv:2012.12304] [INSPIRE].

[112] G. Bell et al., *Effects of Renormalon Scheme and Perturbative Scale Choices on Determinations of the Strong Coupling from e^+e^- Event Shapes*, arXiv:2311.03990 [INSPIRE].

[113] A.H. Hoang, A. Jain, I. Scimemi and I.W. Stewart, *Infrared Renormalization Group Flow for Heavy Quark Masses*, *Phys. Rev. Lett.* **101** (2008) 151602 [arXiv:0803.4214] [INSPIRE].

[114] A.H. Hoang, A. Jain, I. Scimemi and I.W. Stewart, *R-evolution: Improving perturbative QCD*, *Phys. Rev. D* **82** (2010) 011501 [arXiv:0908.3189] [INSPIRE].

JHEP03(2024)123

[115] D. Kang, C. Lee and I.W. Stewart, *Analytic calculation of 1-jettiness in DIS at $\mathcal{O}(\alpha_s)$*, *JHEP* **11** (2014) 132 [arXiv:1407.6706] [INSPIRE].

[116] T. Sjostrand, S. Mrenna and P.Z. Skands, *A Brief Introduction to PYTHIA 8.1*, *Comput. Phys. Commun.* **178** (2008) 852 [arXiv:0710.3820] [INSPIRE].

[117] Z. Chen et al., *Cross Section and Higgs Mass Measurement with Higgsstrahlung at the CEPC*, *Chin. Phys. C* **41** (2017) 023003 [arXiv:1601.05352] [INSPIRE].

[118] G. Cowan, K. Cranmer, E. Gross and O. Vitells, *Asymptotic formulae for likelihood-based tests of new physics*, *Eur. Phys. J. C* **71** (2011) 1554 [*Erratum ibid.* **73** (2013) 2501] [arXiv:1007.1727] [INSPIRE].

[119] J. Alwall et al., *The automated computation of tree-level and next-to-leading order differential cross sections, and their matching to parton shower simulations*, *JHEP* **07** (2014) 079 [arXiv:1405.0301] [INSPIRE].

[120] A.J. Larkoski, S. Marzani, G. Soyez and J. Thaler, *Soft Drop*, *JHEP* **05** (2014) 146 [arXiv:1402.2657] [INSPIRE].

[121] C. Frye, A.J. Larkoski, M.D. Schwartz and K. Yan, *Factorization for groomed jet substructure beyond the next-to-leading logarithm*, *JHEP* **07** (2016) 064 [arXiv:1603.09338] [INSPIRE].

[122] C. Lee, P. Shrivastava and V. Vaidya, *Predictions for energy correlators probing substructure of groomed heavy quark jets*, *JHEP* **09** (2019) 045 [arXiv:1901.09095] [INSPIRE].

[123] S. Ellis, C. Lee, C.K. Vermilion and J.R. Walsh, Unpublished notes.

[124] O.V. Tarasov, A.A. Vladimirov and A.Y. Zharkov, *The Gell-Mann-Low Function of QCD in the Three Loop Approximation*, *Phys. Lett. B* **93** (1980) 429 [INSPIRE].

[125] S.A. Larin and J.A.M. Vermaseren, *The Three loop QCD Beta function and anomalous dimensions*, *Phys. Lett. B* **303** (1993) 334 [hep-ph/9302208] [INSPIRE].

[126] T. van Ritbergen, J.A.M. Vermaseren and S.A. Larin, *The four loop beta function in quantum chromodynamics*, *Phys. Lett. B* **400** (1997) 379 [hep-ph/9701390] [INSPIRE].

[127] T. Gehrmann and D. Kara, *The $Hb\bar{b}$ form factor to three loops in QCD*, *JHEP* **09** (2014) 174 [arXiv:1407.8114] [INSPIRE].

[128] G.P. Korchemsky and A.V. Radyushkin, *Renormalization of the Wilson Loops Beyond the Leading Order*, *Nucl. Phys. B* **283** (1987) 342 [INSPIRE].

[129] S. Moch, J.A.M. Vermaseren and A. Vogt, *The three loop splitting functions in QCD: The Nonsinglet case*, *Nucl. Phys. B* **688** (2004) 101 [hep-ph/0403192] [INSPIRE].

[130] S. Moch, J.A.M. Vermaseren and A. Vogt, *The Quark form-factor at higher orders*, *JHEP* **08** (2005) 049 [hep-ph/0507039] [INSPIRE].

[131] A. Idilbi, X.-D. Ji and F. Yuan, *Resummation of threshold logarithms in effective field theory for DIS, Drell-Yan and Higgs production*, *Nucl. Phys. B* **753** (2006) 42 [hep-ph/0605068] [INSPIRE].

[132] R.V. Harlander and K.J. Ozeren, *Top mass effects in Higgs production at next-to-next-to-leading order QCD: Virtual corrections*, *Phys. Lett. B* **679** (2009) 467 [arXiv:0907.2997] [INSPIRE].

[133] A. Pak, M. Rogal and M. Steinhauser, *Virtual three-loop corrections to Higgs boson production in gluon fusion for finite top quark mass*, *Phys. Lett. B* **679** (2009) 473 [arXiv:0907.2998] [INSPIRE].

JHEP03(2024)123